Journal of Marine Science and Application (2024) 23: 776-797
https://doi.org/10.1007/s11804-024-00477-4

RESEARCH ARTICLE

Hydrodynamic Performance of H-shaped Pile-restrained Floating Breakwater Integrated with Horizontal Plates

Aparna Panda[1], D. Karmakar[1] and Manu Rao[1]

Received: 27 December 2023 / Accepted: 10 March 2024

Abstract

This study analyzes the hydrodynamic performance of an H-shaped pile-restrained composite breakwater integrated with a pair of horizontal plates placed on the seaside and the leeside of the breakwater. The wave interaction with the H-shaped breakwater is examined by analyzing the wave reflection, transmission, and dissipation coefficients. Additionally, the horizontal wave force coefficients are evaluated to analyze the effectiveness of the horizontal plates when integrated with the main structure. The primary structural parameters directly affect the performance of the composite breakwater and are varied within the feasible range of nondimensional wave numbers, relative spacings, and incident wave angles. This study presents a comparative analysis of the arrangement of the horizontal plates in terms of spacing and inclinations inward and outward to the breakwater using a multidomain boundary element method (BEM). The variation of the structural parameters proposes suitable dimensions for integrated H-shaped breakwater with horizontal plates that provide optimal performance in shallow and deep-water regions. The optimum plate porosity, dimensions of the H-shaped structure, inclinations, and spacing between the plate and breakwater are thoroughly discussed. This study shows that impermeable plates are the excellent means to control the wave force in the intermediate water depth regions than in deep-water regions at resisting wave force. The wave force coefficient on the breakwater is significantly larger than that on the seaside plates. Interestingly, inward-inclined plates perform most efficiently at angles greater than 5°, except in deep-water regions where horizontal plates perform better. In addition, this study noted that regardless of water depth, the outward-inclined plates are the least effective in reflecting the incident wave energy. This study will help plan the layout of suitable composite structures for efficient near-shore and offshore harbor protection according to the site criteria and environmental conditions.

Keywords Composite breakwater; Horizontal plates; Reflection and transmission coefficients; Multidomain boundary element method (Multidomain BEM); Wave force coefficient

1 Introduction

Shoreline and harbor protection from wave-induced erosion has become a significant concern in the present day. To address the issue of using heavy structures in deep-water regions and to facilitate the processes of fabrication and transportation, floating breakwaters are considered a modern solution. However, it is important to acknowledge that floating structures may not be able to possess the same level of robustness and strength as traditional rubble mound breakwaters; therefore, floating structures can be integrated with additional wave attenuators, such as barriers and plates, to ensure safety and stability against wave force. The presence of an additional structure can reduce the wave impact on the primary structure by increasing wave energy reflection toward the incident region and can considerably enhance the dissipating wave energy. Studies have been conducted by various researchers on combined structures to analyze their ability to encounter wave attacks and reduce costs at designated locations. Reviews on the basic types of floating breakwaters, along with their installations and corresponding costs, have been discussed by Adee (1976). Studies have proved that the performance of floating breakwaters is closely related to incident wave frequency. The con-

Article Highlights

- The hydrodynamic performance of pile-restrained H-shaped breakwater combined with horizontal/inclined porous plates is analysed using a multidomain boundary element method (BEM).
- Integrating an H-shaped breakwater with a rigid horizontal plate is a useful solution, especially in intermediate water regions where the sea-side plate experiences the least wave force impact.
- Plates on the free surface are more effective in attenuating wave energy than submerged plate.
- Inclining the plates towards the breakwater is more effective in decreasing the impact of waves than placing them horizontally; conversely, an outward inclination promotes less favourable wave interaction.

✉ D.Karmakar
dkarmakar@nitk.edu.in

[1] Department of Water Resources and Ocean Engineering, National Institute of Technology Karnataka, Surathkal, Mangalore 575025, India

cept of implementing floating breakwaters was proposed by Hales (1981) to employ floating structures to counter the reduction of mooring spaces for commercial ships, to reduce the cost of construction in deep-sea deep-water regions and provide a feasible solution for the problem of weak seabed for fixed breakwater foundations. Over the 50 years, various structural parameters for floating breakwaters have been studied by Dai et al. (2018) to improve efficiency and utility of the floating structures as wave attenuating devices. Zhou and Li (2020) reviewed the ongoing and past research and application status of floating breakwaters in terms of wave dissipation and employing new materials and suggested viable key points for their future development.

Research developments on employing various configurations of floating structures, emphasize different shapes of floating structures that can be utilized as breakwaters for efficient wave attenuation. Based on experimental studies under submerged and surface-piercing conditions, Mei and Black (1969) proposed a rectangular shape for traditional breakwaters employed in offshore regions and the study concluded that a variational approach efficiently facilitates the determination of hydrodynamic coefficients of rectangular obstacles. Abul-Azm and Gesraha (2000) examined a rectangular pontoon to analyze a fixed case and a floating case for various incident angles, relative widths, and different drafts using analytical methods. Their findings suggest that, the relative dimension of the cross section of the pontoon greatly influences its wave reflection performance, but its inertial qualities primarily determine its dynamic properties. Additionally, it was determined that the direction of the waves had minmal impact on the reflective properties of the pontoon, especially when the waves formed a wide angle with it. A comparative study was performed by Dong et al. (2008) on single-box, double-box, and board-net type floating breakwaters to optimize the simplest, least expensive, and most effective type of breakwater for deep-water regions based on an experimental study. The study concluded that the board-net floating breakwater, which is simple and inexpensive, can be adopted for aquaculture engineering in deep-water regions. Innovative shapes of floating breakwaters have been the subject of growing interest among researchers to reduce the volume of the structure and to make it cost-efficient in terms of design for the replacement of traditional bulky structures, such as rectangular or trapezoidal shapes. Different floating breakwater configurations, such as T-shaped (Neelamani and Rajendran, 2002a; Zhan et al., 2017; Deng et al., 2019), ⊥-shaped (Neelamani and Rajendran, 2002b; Panduranga and Koley, 2021), U-shaped (Günaydın and Kabdaşlı, 2004), Π-shaped (Günaydın and Kabdaşlı, 2007; Gesraha, 2006), F-shaped (Duan et al., 2016), and H-shaped structures (Neelamani and Vedagiri, 2002), have been analyzed to understand the efficiency and performance of breakwater configurations. Considering the performance based on wave energy reflection and dissipation, T-shaped floating structures are more operational and efficient compared to ⊥-shaped and H-shaped floating structures in dissipating wave energy up to 65% for certain combinations of structural parameters. Recently, the concept of a floating breakwater with an H shape has also proven effective in reducing reflection and transmission coefficients in the case of random waves. Another distinctive shape of a floating breakwater proposed by Ji et al. (2015), i. e., a cylindrical floating breakwater integrated with a flexible mesh cage and several suspending balls, is primarily used to absorb wave energy and convert it into mechanical energy. This innovative configuration is found to be efficient in reducing the transmission coefficient when compared with traditional pontoon-type breakwaters. Zhang and Magee (2021) analyzed the effectiveness of floating breakwaters by combining two or more barges and compared them with traditional breakwaters. The shapes considered for the comparative study were L-shape (two barges), U-shape (three barges), and barge frame (four barges). The transmission characteristics of the above considered shapes suggested that the L-shape floating breakwater is efficient without the presence of floating tanks and that the barge frame is the most efficient in the motion reduction of floating tanks. Nishad et al. (2021) performed a numerical study on wave scattering using an H-shaped porous barriers via a dual boundary element method (BEM) considering the nonlinear pressure-drop boundary condition and analyzed the effect of porosity and geometry of the structure on reducing wave force. Their findings revealed that the increase in the structure porosity results in a consistent increase in wave transmission but a reduction in wave reflection and force coefficients.

In recent years, plate-type floating breakwaters have been investigated for their convenient construction procedure, cost-effectiveness, and invulnerability to depth and geological conditions. Yip and Chwang (2000) designed a model comprising a perforated wall composed of an internal plate to study the hydrodynamic performance using the eigenfunction expansion method and noted that the internal plate helps reduce wave-induced force and moment on the front wall. Hu et al. (2002) conducted a similar kind of study to examine the characteristics of wave transformation on a model that integrated a porous wall with a plate. The investigation revealed that the transmission coefficient of the model is influenced by the porous effect parameter. Liu et al. (2008) investigated a submerged breakwater with an upper horizontal porous plate and a lower horizontal solid plate to analyze the hydrodynamic performance using the matched eigenfunction expansion method. Their investigation suggested that using a perforated lower plate will further enhance the performance of the breakwater. Liu and Li (2013) performed semi-analytical modeling to

study wave interaction with a rubble mound breakwater combined with a plate on its top. The combined use of these two breakwaters yielded better performance than their individual use. Wang et al. (2019) investigated an upper arc-shaped plate using the BEM, considering wave radiation and diffraction theory. The effectiveness of the hydrodynamic performance of the model by minimizing the transmission coefficient to 15%, was determined by comparing it to that of a single horizontal plate, double horizontal plate, and a lower arc-shaped plate. Kumar et al. (2022) used a flexible porous plate combined with a submerged rectangular porous structure to analyse their reflection and transmission characteristics of under oblique incident waves. Particularly for impermeable plates, the presence of the submerged porous structure reduces both the forces acting on the floating plate and the transmission of waves through it, resulting in a more significant reduction in plate deflection. Further, they noted that the existence of the plate is helpful in force mitigation of the rubble mound breakwater and in wave transmission.

Studies on stratified structures have been performed over the past 30 years to address the problems of cost-inefficiency and material scarcity associated with submerged and floating breakwaters. Yu and Chwang (1994) analysed the horizontal stratification of breakwaters considering nondissipative, weak-dissipative, and strong-dissipative media. Moreover, they studied interface wave interaction considering the resistive and inertial properties of these media; the results of their study suggested an optimum thicknes for the porous structure to effectively reduce transmission and reflection. Further, Twu et al. (2001) performed a numerical investigation on a series of vertically stratified breakwaters with multiple porosities in deep water, while Liu et al. (2007) studied modified perforated structures in which a double-layered porous box was connected with two walls on both sides. The hydrodynamic performances of these breakwaters were analysed, and it was found that the hydrodynamic performances of the perforated breakwaters with two- or single-layer surface-piercing rock fill were similar. Koley (2019) performed a hydrodynamic study under regular- and irregular-wave conditions for a trapezoidal porous stratified structure in a surface-piercing condition and observed that a multilayer structure is most effective for the protection of the lee side of the trapezoidal porous stratified structure and can serve as an effective wave barrier. Venkateswarlu and Karmakar (2020) studied multiple vertical and horizontal stratified structures and analysed the effect of porosity, friction factor, oblique incident waves, and different structural parameters on reflected, transmitted, and dissipated wave energy coefficients and wave forces. Design and development of stratified porous wave absorbers for the protection of marine infrastructure is assisted by the harmonic oscillations and peaks and troughs in the trapping coefficients that are demonstrated by the change in trapping chamber length. The cavitation effect impacts the functionality and stability of any structure owing to the negative pressure induced in the bubble, which is thoroughly discussed by Zhang et al. (2023) considering rigid and free surface boundaries.

The present study considers a composite structure of an H-shaped pile-restrained floating breakwater integrated with a pair of horizontal plates both on the lee side and seaside using the multidomain BEM. Based on the studies performed by Liu and Li (2013), horizontal plates are believed to confront the primary impact of the incident wave force by reducing the wave force transmitted to the breakwater. The H-shaped breakwater exhibits excellent wave energy reflection as a floating breakwater compared with conventional rectangular and trapezoidal breakwaters. An H-shaped breakwater is modeled in the present study to enhance the performance of breakwaters, considering their cost-effectiveness and easy installation. Findings from the literature suggest that the vertical member of an H-shaped structure, designated as the "web," serves as a physical barrier and promotes capillary action across its entire surface area, thereby amplifying wave reflection. Conversely, the horizontal member, called the "flange," creates an internal wave-trapping zone within the unit structure, significantly mitigating wave transmission. The porosity of the H-shaped structure promotes capillary action (Leverett, 1941), further enhancing the wave-trapping zone and thereby reducing the wave transmission and dissipation of high-energy waves. Additional safety and stability need to be provided to the composite structures to make the primary floating breakwater safe against wave force and resistant to the damage caused by incoming wave energy. Hence, the motivation of the present study is to establish the excellence of an H-shaped breakwater integrated with horizontal plates, evaluate its performance in minimizing the amount of wave energy that reaches the coastline, and understand the behavior of the breakwater according to the quantitative and qualitative changes in wave reflection and transmission. The present study involves measuring the wave dissipation parameters and wave force against nondimensional wave numbers, relative spacings, and incident wave angles affected by the presence of the plates. Further, the validation of the developed numerical model is performed using notable results from the literature.

2 Theoretical formulation

The hydrodynamic performance of the H-shaped breakwater combined with two horizontal porous plates on both sides of the breakwater is performed using the multidomain BEM. An ideal geometry of the proposed model is presented in Figure 1 showing different structural and physical parameters, boundaries for fluid, and structural elements. In addi-

tion, Figure 1 represents the arrangement of the porous structures (i.e., H-shaped breakwater and horizontal plates) of the proposed model with corresponding intra-structure spacing. The numerical formulation of the wave–structure interaction with the H-shaped breakwater integrated with horizontal plates is performed, and the detailed mathematical procedure using the multidomain BEM (Patil and Karmakar, 2021) is presented. The fluid flow is assumed to be inviscid, incompressible, and irrotational, and thus, the velocity potential (ϕ) for an obliquely incident wave is of the form, $\phi(x, y, z, t) = \mathrm{Re}\left\{\phi(x, y)e^{i(k_z - \omega t)}\right\}$, where $k_z = k\sin\theta$, k is the wave number, θ is the angle of incident wave; ω is the angular wave frequency; i is the imaginary number. The velocity potential satisfies the Helmholtz equation in the fluid domain Ω, which can be expressed as follows:

$$\left(\nabla^2 - k_z^2\right)\phi(x,y) = 0 \text{ for the fluid domain } \Omega \tag{1}$$

where ∇ is the Laplace operator.

Considering the fluid domain Ω, Γ_{SB} represents the sea-bed region, Γ_{STR} represents the structure-fluid interface, and Γ_{FS} represents the free surface region. The fluid is assumed to flow from the negative x-axis to the positive x-axis. Hence, the input and output open boundary regions are denoted by Γ_{INPUT}, Γ_{OUTPUT}, respectively. More precisely, Γ_{INPUT} indicates the incident region, and Γ_{OUTPUT} indicates the transmitted region.

The free-surface Γ_{FS} boundary condition based on Bernoulli's equation, where the wave amplitudes are assumed small, is given by

$$\frac{\partial\phi}{\partial y} - \frac{\omega^2}{g}\phi = 0 \tag{2}$$

where g represents the acceleration due to gravity; given an impervious horizontal sea-bed Γ_{SB}, which is assumed to be flat and impermeable, the sea-bed boundary condition is of the form

$$\frac{\partial\phi}{\partial y} = 0 \text{ at } y = -h \tag{3}$$

where h represents the water depth. The porous structure interacts with the fluid region surrounding each surface, forming a fluid-structure interface. Hence, to maintain the continuity of mass flow and pressure at the interfaces (Dalrymple et al., 1991), the matching condition is given by

$$\frac{\partial\phi^f_{STR}}{\partial n} = -\varepsilon\frac{\partial\phi^s_{STR}}{\partial n}\ ,\ \phi^f_{STR} = (S + if)\phi^s_{STR} \tag{4}$$

where ϕ^f_{STR} is the velocity potential in the water region and ϕ^s_{STR} is the velocity potential in the structural region, and the relation among the boundaries at the interfaces can be established by material porosity ε, linearized friction factor f, and inertia coefficient S.

The structure is assumed to be situated between the two auxiliary boundaries Γ_{INPUT} and Γ_{OUTPUT} from the structure on each side. Therefore, the far-field radiation condition for input and output open boundary conditions is given by

$$\lim_{n\to\infty}\sqrt{r}\left(\frac{\partial\phi}{\partial r} - ik\phi\right) = 0 \tag{5}$$

where r represents the distance between the point source and radial coordinates, and $r = \sqrt{x^2 + y^2}$. The velocity potential function at the input and output boundaries can be expressed as follows:

$$\phi_{INPUT} = \phi_I + \phi_R\,,\ \phi_{OUTPUT} = \phi_T \tag{6}$$

where ϕ_I is the velocity potential for the incident wave, ϕ_R is the velocity potential for the reflected wave, and ϕ_T is the velocity potential for the transmitted wave. According to the small-amplitude wave theory, the velocity potential functions can be expressed as follows:

$$\phi_{INPUT} = \frac{iag}{\omega}\left[I_0e^{ikx} + R_0e^{-ikx}\right]f_0(y),\ x\to\infty \tag{7a}$$

$$\phi_{OUTPUT} = \frac{iag}{\omega}\left[T_0e^{ikx}\right]f_0(y),\ x\to-\infty \tag{7b}$$

where a is the wave amplitude, I_0 is the unknown potentials associated with incident potentials, and similarly R_0

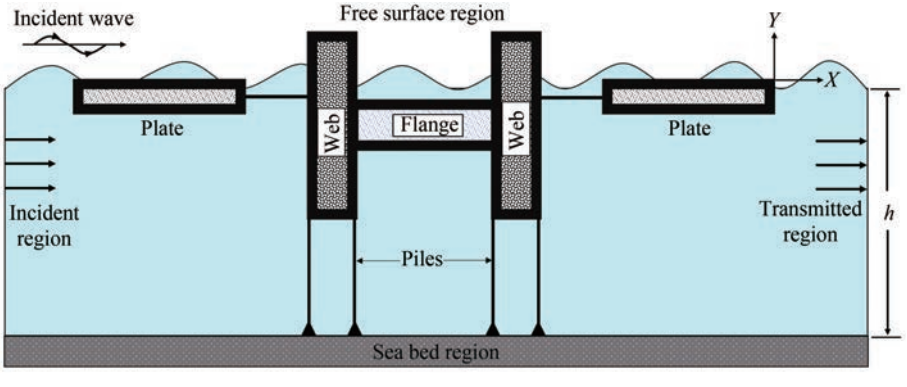

Figure 1 Schematic diagram of an H-shaped breakwater integrated with a pair of floating plates

and T_0 are the unknown potentials associated with reflected and transmission potentials respectively, and the function $f_0(y)$ is given by

$$f_0(y) = \frac{\cosh k(h+y)}{\cosh kh} \tag{8}$$

The wave number k and the angular wave frequency ω satisfy the dispersion relation

$$\omega^2 = gk\tanh kh \tag{9}$$

The boundary conditions for the composite H-shaped breakwater integrated with floating plates for the analysis of wave interaction with floating breakwaters are discussed in the next section.

3 Method of solution using multidomain BEM

The multidomain BEM approach is employed to analyse the wave interaction with an H-shaped breakwater integrated with floating plates. The fundamental solution of the governing equation satisfies the relation given by

$$\nabla^2 G - k_z^2 G = \delta(\xi - x, \eta - y) \tag{10}$$

where δ is the dirac-delta function; k_z is the vertical component of the wave number; (x, y) are the coordinates of field points and (ξ, η) are the coordinates of source point respectively. G is free surface Green's function, which can be represented as follows:

$$G(x, y, \xi, \eta) = \frac{-K_0(k_z, r)}{2\pi} \tag{11}$$

where $r = \sqrt{(x-\xi)^2 + (y-\eta)^2}$ is the distance between the field point $F(x, y)$ and the source point $P(\xi, \eta)$. The term K_0 is the modified zeroth-order Bessel function of the second kind. The normal derivative of Green's function is given as

$$\frac{\partial G}{\partial n} = \frac{k_z}{2\pi} K_1(k_z r)\frac{\partial r}{\partial n} \tag{12}$$

where n refers to the outward drawn normal; K_1 is the modified first-order Bessel function of the second kind, and in the case of singularity $r \to 0$, the asymptotic behavior of K_0 is given by

$$K_0(k_z r) = -\gamma - \ln\left(\frac{k_z r}{2}\right) \tag{13}$$

where $\gamma = 0.577\,2$ is the Euler's constant. Furthermore, in the case of normal incident wave angle $\theta = 0$, the modified zeroth-order Bessel function of the second kind $K_0(k_z r)$ approaches to $-\ln(r)$. The generalized form of the boundary integral equation, considering free-space Green's function and applying Green's second identity, is represented as

$$c(P)\phi + \int_\Gamma \phi \frac{\partial G}{\partial n} \mathrm{d}\Gamma = \int_\Gamma G \frac{\partial \phi}{\partial n} \mathrm{d}\Gamma \tag{14}$$

where Γ denotes the boundary of the computational domain under consideration; $c(P)$ is denoted by

$$c(P) = \begin{cases} 1\,,\ P \equiv (\xi, \eta) \in \Omega \\ \dfrac{1}{2}, P \equiv (\xi, \eta) \in \Gamma \text{ is smooth} \\ 0\,,\ P \equiv (\xi, \eta) \in \Omega, \Gamma \end{cases} \tag{15}$$

where P is the source point Thus, the final boundary integral equation can be represented as

$$\frac{\phi(P)}{2} + \int_\Gamma \frac{\partial G}{\partial n}\phi \mathrm{d}\Gamma = \int_\Gamma \frac{\partial \phi}{\partial n} G \mathrm{d}\Gamma \tag{16}$$

The boundary is divided into N number of constant elements, and the values of ϕ and G are considered as constant over each element and assumed to be equal at the mid-element node. Hence, Equation (16) is discretised into N constant boundary elements, and the discretised boundary integral equation can be expressed as

$$\frac{\phi(P)}{2} + \sum_{j=1}^{N}\left(\int_{\Gamma_j} \frac{\partial G}{\partial n}\phi_j \mathrm{d}\Gamma\right) = \sum_{j=1}^{N}\left(\int_{\Gamma_j} \frac{\partial \phi}{\partial n} G_j \mathrm{d}\Gamma\right) \tag{17}$$

where Γ_j is the boundary of the jth element. Considering $\int_{\Gamma_j} \frac{\partial G}{\partial n}\mathrm{d}\Gamma = H_{ij}$ and $\int_{\Gamma_j} \mathrm{G}_j \mathrm{d}\Gamma = Q_{ij}$, the expression for the boundary integral equation as in Equation (17) is given by

$$-\frac{\phi(P)}{2} + \sum_{j=1}^{N}\left(H_{ij}\phi_j\right) = \sum_{j=1}^{N}\left(Q_{ij}\frac{\partial \phi}{\partial n}\right) \tag{18}$$

The boundaries for the fluid and structural regions and fluid-structure interfaces are briefly described in Figure 2.

The integrals in H_{ij} and G_{ij} represent the influence functions between the element i at which the fundamental solution is applied and another element j under consideration (Patil and Karmakar, 2021). The corresponding dimensions and physical properties are substituted in the boundary conditions for the plates and breakwater regions while interacting with fluid, free surface, and seabed accordingly. On substituting the boundary conditions, the expanded discretized equation can be written for the fluid region as

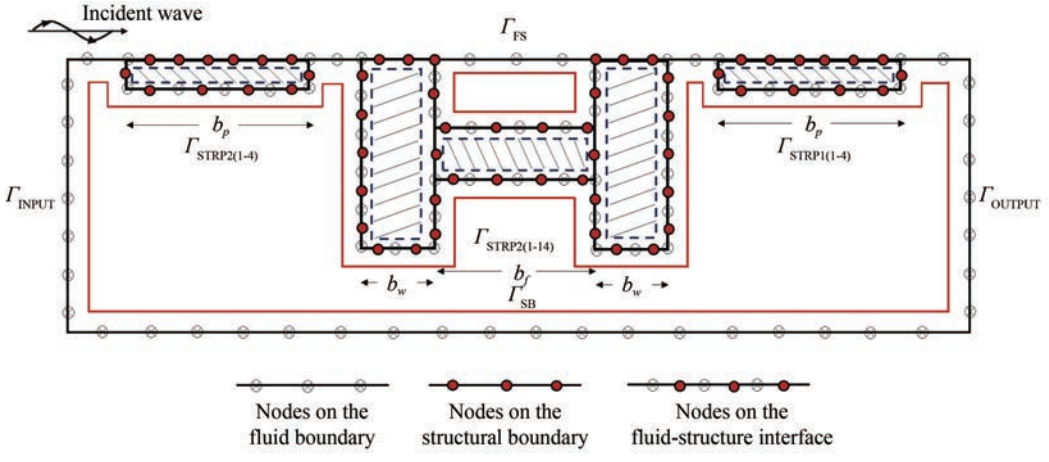

Figure 2 Boundary elements for fluid and structure boundaries

$$\frac{1}{2}\phi_{\mathrm{R}}^{\mathrm{f}}+\sum_{j=1}^{N}\left(H_{ij}\phi_{\mathrm{SB}}^{\mathrm{f}}\right)+\sum_{j=1}^{N}\left(H_{ij}-\mathrm{i}kQ_{ij}\right)\phi_{\mathrm{OUTPUT}}^{\mathrm{f}}+\sum_{j=1}^{N}\left(H_{ij}-\frac{\omega^2}{g}Q_{ij}\right)\phi_{\mathrm{FS1}}^{\mathrm{f}}+\sum_{j=1}^{N}\left(H_{ij}\phi_{\mathrm{STRP1}}^{\mathrm{f}}\right)-\sum_{j=1}^{N}\left(Q_{ij}\frac{\partial\phi_{\mathrm{STRP1}}^{\mathrm{f}}}{\partial n}\right)+\sum_{j=1}^{N}\left(H_{ij}-\frac{\omega^2}{g}Q_{ij}\right)\phi_{\mathrm{FS2}}^{\mathrm{f}}+\sum_{j=1}^{N}\left(H_{ij}\phi_{\mathrm{STR}}^{\mathrm{f}}\right)-\sum_{j=1}^{N}\left(Q_{ij}\frac{\partial\phi_{\mathrm{STR}}^{\mathrm{f}}}{\partial n}\right)+\sum_{j=1}^{N}\left(H_{ij}-\frac{\omega^2}{g}Q_{ij}\right)\phi_{\mathrm{FS3}}^{\mathrm{f}}+\sum_{j=1}^{N}\left(H_{ij}\phi_{\mathrm{STRP2}}^{\mathrm{f}}\right)-\sum_{j=1}^{N}\left(Q_{ij}\frac{\partial\phi_{\mathrm{STRP2}}^{\mathrm{f}}}{\partial n}\right)+\sum_{j=1}^{N}\left(H_{ij}-\frac{\omega^2}{g}Q_{ij}\right)\phi_{\mathrm{FS4}}^{\mathrm{f}}+\sum_{j=1}^{N}\left(H_{ij}-\mathrm{i}kQ_{ij}\right)\phi_{\mathrm{INPUT}}^{\mathrm{f}}=0 \tag{19}$$

and considering the structural region (i.e., the plates and breakwater region), the discretized equations for the lee-side plate, breakwater and sea-side plate are given by

$$-\frac{1}{2}\phi^{\mathrm{s}}+\sum_{j=1}^{N}\left(H_{ij}\phi_{\mathrm{STRP1}}^{\mathrm{s}}\right)-\sum_{j=1}^{N}\left(Q_{ij}\frac{\partial\phi_{\mathrm{STRP1}}^{\mathrm{s}}}{\partial n}\right)=0 \tag{20}$$

$$-\frac{1}{2}\phi^{\mathrm{s}}+\sum_{j=1}^{N}\left(H_{ij}\phi_{\mathrm{STR}}^{\mathrm{s}}\right)-\sum_{j=1}^{N}\left(Q_{ij}\frac{\partial\phi_{\mathrm{STR}}^{\mathrm{s}}}{\partial n}\right)=0 \tag{21}$$

$$-\frac{1}{2}\phi^{\mathrm{s}}+\sum_{j=1}^{N}\left(H_{ij}\phi_{\mathrm{STRP2}}^{\mathrm{s}}\right)-\sum_{j=1}^{N}\left(Q_{ij}\frac{\partial\phi_{\mathrm{STRP2}}^{\mathrm{s}}}{\partial n}\right)=0 \tag{22}$$

where the superscript s is for the porous structure domain

The revised discretized equation on substituting the input and output velocity potentials as in Equation (7) can be expressed for the fluid region as

$$-\frac{1}{2}\phi_{\mathrm{R}}^{\mathrm{f}}+\sum_{j=1}^{N}\left(H_{ij}\phi_{\mathrm{SB}}^{\mathrm{f}}\right)+\sum_{j=1}^{N}\left(H_{ij}-\mathrm{i}kQ_{ij}\right)\phi_{\mathrm{OUTPUT}}^{\mathrm{f}}+\sum_{j=1}^{N}\left(H_{ij}-\frac{\omega^2}{g}Q_{ij}\right)\phi_{\mathrm{FS1}}^{\mathrm{f}}+\sum_{j=1}^{N}\left(H_{ij}\phi_{\mathrm{STRP1}}^{\mathrm{f}}\right)-\sum_{j=1}^{N}\left(Q_{ij}\frac{\partial\phi_{\mathrm{STRP1}}^{\mathrm{f}}}{\partial n}\right)+\sum_{j=1}^{N}\left(H_{ij}-\frac{\omega^2}{g}Q_{ij}\right)\phi_{\mathrm{FS2}}^{\mathrm{f}}+\sum_{j=1}^{N}\left(H_{ij}\phi_{\mathrm{STR}}^{\mathrm{f}}\right)-\sum_{j=1}^{N}\left(Q_{ij}\frac{\partial\phi_{\mathrm{STR}}^{\mathrm{f}}}{\partial n}\right)+\sum_{j=1}^{N}\left(H_{ij}-\frac{\omega^2}{g}Q_{ij}\right)\phi_{\mathrm{FS3}}^{\mathrm{f}}+\sum_{j=1}^{N}\left(H_{ij}\phi_{\mathrm{STRP2}}^{\mathrm{f}}\right)-\sum_{j=1}^{N}\left(Q_{ij}\frac{\partial\phi_{\mathrm{STRP2}}^{\mathrm{f}}}{\partial n}\right)+\sum_{j=1}^{N}\left(H_{ij}-\frac{\omega^2}{g}Q_{ij}\right)\phi_{\mathrm{FS4}}^{\mathrm{f}}+\sum_{j=1}^{N}\left(H_{ij}-\mathrm{i}kQ_{ij}\right)\phi_{\mathrm{R}}^{\mathrm{f}}=-\sum_{j=1}^{N}\left(H_{ij}-\mathrm{i}kQ_{ij}\right)\phi_{\mathrm{I}}^{\mathrm{f}} \tag{23}$$

The indication of superscript f is for the fluid region. The interface boundaries for both fluid and structure regions have the same potential ϕ_{STRj}^{m} and flux $\partial\phi_{\mathrm{STRj}}^{m}/\partial n$ on the boundary. It is assumed that the structure-sea-bed interface and structure-free surface interface are rigid. Hence, the flux is given by

$$\frac{\partial\phi_{\mathrm{STRj}}^{m}}{\partial n}=0 \tag{24}$$

To solve the system of linear equations, the matching boundary conditions are applied to get the unknown potentials ϕ_{I}, ϕ_{R} and ϕ_{T}. The system of equations is solved by the Gauss-elimination technique. Furthermore, the reflection coefficient K_{r}, transmission coefficient K_{t}, and dissipation coefficient K_{d} are calculated as

$$K_r = \left|\frac{R_0}{I_0}\right|, K_t = \left|\frac{T_0}{I_0}\right|, K_d = \sqrt{1 - K_r^2 - K_t^2} \quad (25)$$

The horizontal and vertical wave forces acting on the structure are determined by the relation as defined by Koley (2019) and can be written as

$$\boldsymbol{F} = \mathrm{Re}\left[\mathrm{i}\rho\omega \int_{\Gamma_{\mathrm{STR}J}} \begin{bmatrix} n_x \\ n_y \end{bmatrix} \phi_{\mathrm{STR}} \mathrm{d}\Gamma\right] \quad (26)$$

$\boldsymbol{F}$ can be expressed as $\boldsymbol{F} = \begin{bmatrix} F_x \\ F_y \end{bmatrix}$, where n_x and n_y are the unit normal vectors in the x- and y-direction on Γ_{STR}, respectively.

4 Numerical results and discussion

The hydrodynamic analysis is performed for wave interaction with a composite pile-restrained H-shaped floating breakwater integrated with a pair of floating plates using the multidomain BEM. The numerical study is performed for the detailed analysis of the effect of the variation of various structural parameters (such as porosity, width, and submergence draft) on the wave-energy reflection, transmission, and dissipation coefficients, as well as wave force coefficients. The hydrodynamic coefficients are measured as functions of nondimensional wave number, relative spacing, and wave incident angle. The numerical modeling based on the multidomain BEM is implemented in MATLAB, and the numerical results from the simulations are validated with the existing literature. The study also covers a short comparative study between the implementation of inward and outward inclined horizontal plates integrated with the breakwater.

4.1 Validation of the numerical model

The validation of the numerical code developed using the multidomain BEM in this study is performed with the numerical model proposed by Abul-Azm and Gesraha (2000) for a rigid floating pontoon (Figure 3(a)) and a horizontally stratified structure studied by Yu and Chwang (1994) (Figure 3(b)). The physical parameters used to validate the model of Abul-Azm and Gesraha (2000) are incidence angle $\theta = 0$, relative water depth $d/h = 0.25$, and relative width $B/h = 2$. where I is the incident wave amplitude, R is the reflected wave amplitude and T is the transmitted wave amplitude. A satisfactory agreement of the reflection and transmission coefficients versus nondimensional wave number kh is observed between the present multidomain BEM model and the result obtained by Abul-Azm and Gesraha (2000) in Figure 3(a). The study concludes that the relative dimensions of the cross-sections of a pontoon have significant effects on wave reflection, whereas the impact of wave direction is minimal for higher wave incident angles. Additionally, it has been noted that the inertial characteristics affect the dynamic properties of the model. Due to the satisfactory agreement of the results obtained from the present multidomain BEM with the study performed by Abul-Azm and Gesraha (2000), the multidomain BEM study is carried out for the pile-restrained H-shaped breakwater integrated with plates.

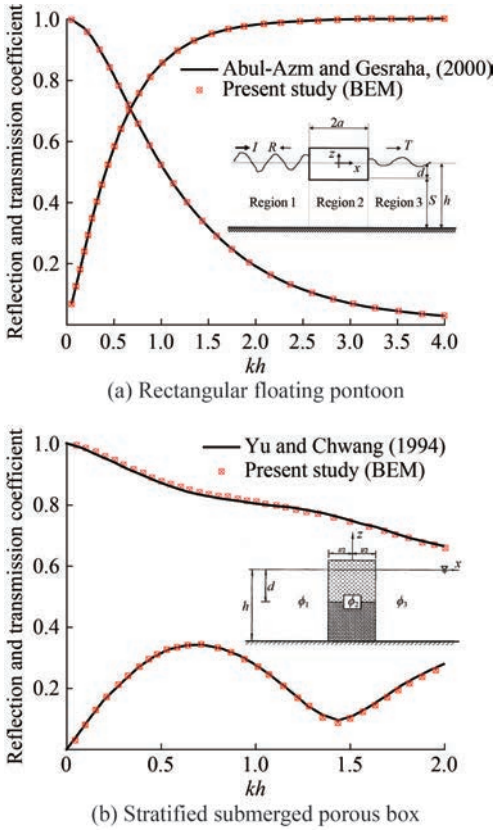

Figure 3 Comparative study of reflection coefficient K_r and transmission coefficient K_t for a rectangular floating pontoon using the multidomain BEM approach by Abul-Azm and Gesraha (2000) and a stratified submerged porous box of different porosity values using the multidomain BEM approach by Yu and Chwang (1994)

Furthermore, the wave interaction with horizontal stratified structure in Figure 3(b) is validated by Yu and Chwang (1994) using the present multidomain BEM approach, considering $\varepsilon_1 = \varepsilon_2 = 0.8$, $S_1 = S_2 = 0.2$, and $f_1 = f_2 = 2$. The study noted that lowering the porosity results in higher reflection and lower transmission in a structure, which is efficient in energy dissipation. The study also suggests that wave dissipation occurs when it transmits into a medium that has a significant value of porosity and decreases when porosity decreases. The numerical result using the present multidomain BEM approach and the Eigenfunction expansion method (EFEM) for stratified structure modeled by Yu and Chwang (1994) are in good agreement, and the multidomain BEM approach is extended for the study.

4.2 H-shaped pile-restrained floating breakwater with horizontal plates

The H-shaped floating breakwater facilitates efficient dissipation of wave energy in various wave conditions and site requirements. In addition, the H-shaped floating breakwater is advantageous for shore protection and is flexible to fabricate, construct, and transport in deep-water regions. The vertical and horizontal components of an H-shaped structure are efficient in dispersing the wave energy by reflecting the incoming waves, but a study on the performance of the structure is required. Hence, the integration of a plate in the lee side and seaside of the breakwater is a unique approach to increase the performance of the structure against wave forces in unfavorable environmental conditions. This study explores the combined effect of the H-shaped breakwater and the plates on the incoming waves from various structural parameters and incident wave angles. Table 1 presents the structural and geometrical parameters considered for the present analysis of the composite breakwater.

The numerical investigation is performed to analyze the reflection, transmission, and dissipation coefficient for various physical and structural parameters, such as porosity of plates ε_p, relative plate submergence depth d_p/h (d_p is the submergence draft of the plate measured from the free surface), relative submergence draft of the breakwater d_w/h (d_w is the submergence draft of web measured from free surface), relative breakwater widths b_w/h and b_f/h (b_w and b_f represent the width of the web and flange of a single monomer), and angles of inclination of the horizontal plates for outward direction a_{po} and inward direction a_{pi} to analyze the effectiveness toward the efficiency and performance of the best suitable structure. The relative width of the spacing between the plates and breakwater $w_s/h = 1$ is assumed to be constant throughout the analysis. The values of the structural parameters kept constant throughout the analysis are presented in Table 1 unless otherwise mentioned.

4.2.1 Reflection, transmission, and dissipation coefficients

The performance of offshore structures can be analyzed by studying the wave transformation resulting from the wave–structure interactions. The stability and optimal protection of the breakwater depend on the extent of reflected or transmitted wave energy. The study of the variations of the hydrodynamic coefficients presents the idea of the amount of wave energy reflected by the structure, transmitted through the porous region, and dissipated during the interaction. The effects of changing different structural and physical parameters can be analyzed for the suitable shape of the breakwater and the installation based on the site conditions from various aspects of wave behavior and environmental conditions. Various offshore structure designs and coastal management applications rely on structural performance evaluation and model validations, which can only be accomplished by the study of the hydrodynamic wave transformation and force coefficients. This study analyzes the possible structural parameters related to the present composite H-shaped breakwater integrated with plates on varying nondimensional parameters, such as wave number kh, relative spacing w_s/λ (λ represents the wavelength), and incident wave angle θ.

4.2.1.1 Effect of plate porosity

Figures 4(a) and (b) illustrate the variation of the reflection coefficient K_r, transmission coefficient K_t, and dissipation coefficient K_d versus the nondimensional wave number kh for different ranges of porosities within the range $0 \leqslant \varepsilon_p \leqslant 0.3$. The study revealed that the effect is insignificant in shallow and intermediate-water-depth regions $(kh \leqslant 2.0)$. Unlike other breakwater configurations, the H-shaped structure, with its efficient flange-based wave trapping, ensures minimal transmission regardless of porosity variations, particularly in deep-water regions, in contrast to K_r and K_d.

Table 1 Structural parameters for different configurations

Structural configurations	Porosity	Friction factor	Inertia factor	Relative width	Relative draft
Plates 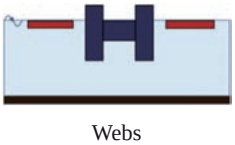	$\varepsilon_p = 0.1$	$f_p = 1$	$S_p = 1$	$b_p/h = 1.0$	$d_b/h = 0.1$
Webs 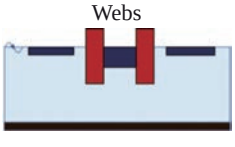	$\varepsilon_w = 0.1$	$f_w = 1.2$	$S_w = 1$	$b_w/h = 0.3$	$d_w/h = 0.3$
Flange 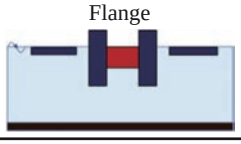	$\varepsilon_f = 0.2$	$f_f = 1$	$S_f = 1$	$b_f/h = 1.6$	$d_f/h = 0.1$

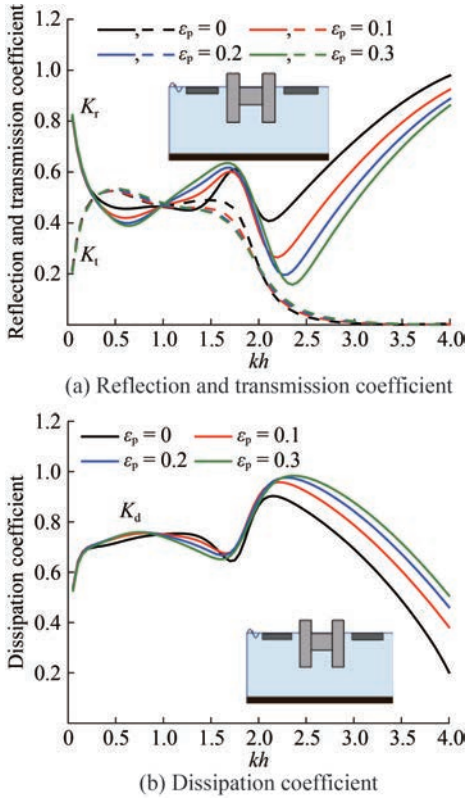

Figure 4 Variation of reflection, transmission, and dissipation coefficient versus kh for different porosity of plates ε_p

Considering the reflection property due to the composite structure (Figure 4(a)), the lesser porous structure has higher reflection, and the rigid plate approaches 100% reflection in the deep-water region ($kh \geqslant 3.14$). Likewise, the impermeability in the plate promotes lower energy dissipation (Figure 4(b)) when the wave interacts with the composite type of structure. Hence, the variation of plate porosity has a lesser effect on the wave propagation through the composite structure due to the less effective obstruction as the thickness of the plate is assumed as $d_p/h = 0.1$. The K_r (Figure 4(a)) and K_d (Figure 4(b)) have an insignificant oscillatory pattern as the wave energy interacts with a set of structures with a significant structural spacing in between. The wave energy dissipated by the structure is lowest, regardless of the porosity variation of the plate in deep-water regions ($kh \geqslant 3.14$). In deep-water regions, higher plate porosity in H-shaped breakwaters leads to more energy dissipation due to the combined effect of obstruction due to the presence of horizontal plates and wave trapping. Hence, the composition of horizontal plates with an H-shaped breakwater is advantageous in lowering wave transmission (Hu et al., 2002) and can be implemented in deep-water regions.

The performance of different plate porosity values is analyzed based on varying the relative spacing between the breakwater and plates in Figures 5(a) and 5(b). A significant oscillatory pattern is observed in the variation of K_r, K_t, and K_d versus the nondimensional wave number kh, for different porosity values of plates varying within $0 \leqslant \varepsilon_p \leqslant 0.3$, due to the presence of multiple structures in the wave interaction. The periodic variation in the reflection and transmission coefficients is caused by varying the porosity of the plates of the composite structure. Comparing the variation of K_t (Figure 4(a)) with wave number, the variation of K_t (Figure 5(a)) with relative spacing has minimal effect due to the variation of plate porosity. The peak in K_t followed by a trough is attained by the variations of plate porosity for every $w_s/\lambda = 2.0$. Due to the impermeability of the plate ($\varepsilon_p = 0$), the composite structure provides a better reflection coefficient and lower transmission coefficient compared with those of other porous structures, with the lowest energy dissipation observed between $1.0 \leqslant w_s/\lambda \leqslant 3.0$. The plate with $\varepsilon_p = 0.3$ dissipates the maximum amount of wave energy up to 98% due to the wave trapping in porous structures, which is further enhanced by the variation of inter-spacing within the composite structure. The optimum range of inter-structural spacing is denoted by $w_s/\lambda = 2.5$ for the plate with higher porosity, which yields better wave reflection by dissipating lower energy. Hence, the inter-structural spacing can be considered in field applications for the efficient performance of the composite breakwater.

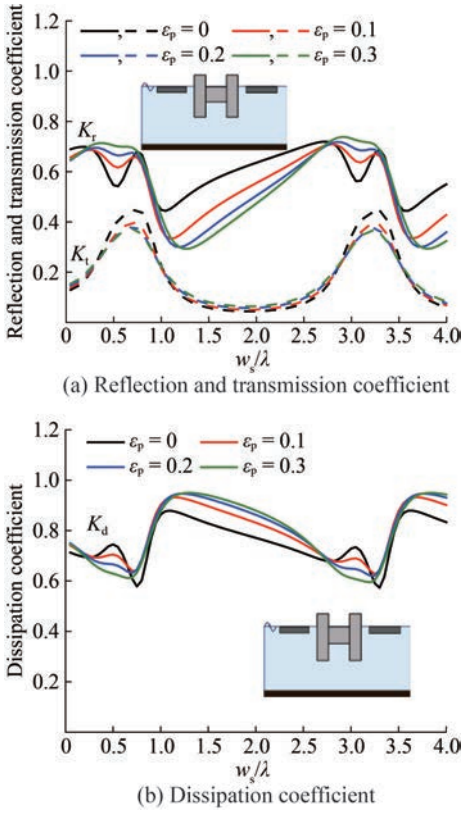

Figure 5 Variation of reflection, transmission, and dissipation coefficients versus w_s/λ for different plate porosities ε_p

Figures 6(a) and 6(b) represent the wave transformation due to the composite H-shaped breakwater integrated with floating plates, in terms of reflection, transmission, and dissipation coefficients versus different wave incident angles within $0° \leqslant \theta \leqslant 90°$. The plate porosities are considered within $0 \leqslant \varepsilon_p \leqslant 0.3$ for nondimensional wave number $kh = 2$. The energy dissipation coefficient (Figure 6(b)) is noted to approach zero as the dissipated energy decreases with higher wave incident angles ($\theta \geqslant 50°$). A sudden minima or maxima in the variations of K_r, K_t, and K_d is observed within $40° \leqslant \theta \leqslant 60°$. In the case of wave incidence angle $\theta = 90°$, the reflection is noted maximum with almost 100% of wave reflection. Waves with the incident angle $\theta < 40°$ is noted to have reflection coefficients within $0.6 < K_r < 0.8$ until it reaches the critical incident angle. In the study, the critical angle of incidence for the lowest reflection coefficient and highest transmission coefficient is found to be within $40° \leqslant \theta \leqslant 60°$, which also has significance in dissipating the highest energy. Except for the critical incident angle range, the transmission coefficient is almost zero for any case of porosity variation (Figure 6(a)). The impermeability of the plates may be the reason to reflect more energy and dissipate less energy at lower wave incident angles. The deployment of horizontal porous plates within the critical angle range could potentially result in a less efficient breakwater due to enhanced wave energy transmission. Further analysis can be performed to determine the ideal dimensions of the composite structure and inclination of plates for efficient performance under the critical wave incident angle.

4.2.1.2 Effect of submergence depth of plates

The integration of plates with an H-shaped breakwater exhibits higher wave energy dissipation with the change in the porosity of the plate on varying hydrodynamic coefficients. Thus, the idea of placing the plates in submerged condition is studied to analyze the performance of the composite breakwater. Figures 7(a) and 7(b) show the variation of hydrodynamic coefficients K_r, K_t and K_d versus nondimensional wave number kh to study the effect of changing the relative submergence depth of the plates from the free surface within $0 \leqslant d_{sp} \leqslant 0.3$ in different water depth regions. Initially, the numerical model is analyzed by placing the plate on a free surface, and then, the submergence of the plates is increased and compared. Throughout the relative submergence depth comparison of plates, the submergence draft of the webs is placed deeper, i.e., $d_w/h \geqslant d_{sp}/h$. The plate positioned at the free surface exhibits higher values of K_r (Figure 7(a)) and lower values of K_d (Figure 7(b)) for all water depth regions compared to any case of submerged plates. The higher K_t observed for submerged plates may be due to the placement of the plates below the free surface, allowing the wave energy to escape with a free passage instead of reflecting back. However, K_r shows an inverse relationship with d_{sp}/h in the intermediate-water-depth region $0.3 \leqslant kh \leqslant 1.5$ (Figure 7(a)), and the noted difference is significant with the variation in d_{sp}/h as the water depth increases.

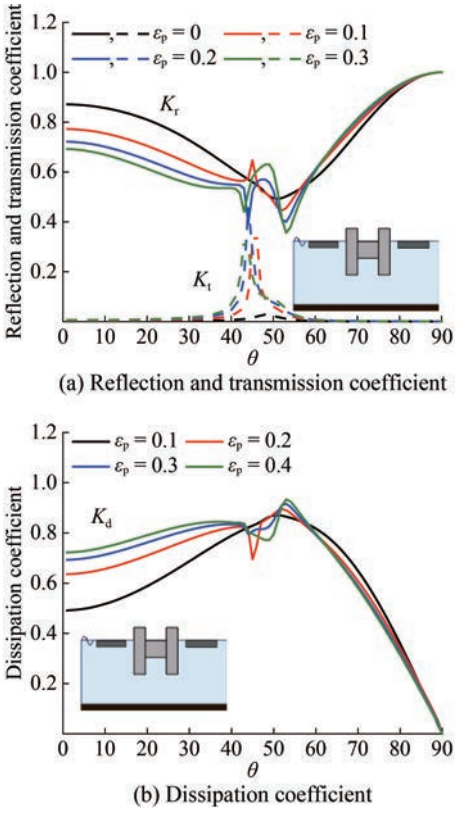

Figure 6 Variation of reflection, transmission, and dissipation coefficients versus θ for different plate porosities ε_p

Similar to the results in in Figure 7(b), the dissipated energy is higher for lower d_{sp}/h considering the intermediate-water-depth region. A sudden fall is observed in the intermediate-water-depth region due to the higher reflected wave energy variation resulting from the plate at the free surface, which obstructs the smooth passage of waves. The presence of plates at the free surface effectively blocks the smooth passage of waves, unlike other submergence depths where waves pass over the plates, resulting in lower transmission. Since energy dissipation is directly related to the reflection and transmission coefficients, the wave dissipation experiences a sudden dip at this specific depth. Thus, the energy dissipation is raised for submerged plates as this restricts the reflection due to the water body around the plates with a low d_{sp}/h. Considering the transmission properties through the composite body, in the shallow and intermediate-water-depth regions ($kh \leqslant 1.5$), the H-shaped breakwater with plates at the free surface has a higher rate of K_t than the submerged plates ($d_{sp}/h \geqslant 0.1$). However, as the water depth increases, the resulting submerged plates transmit higher values of wave energy. The maximum rate of transmission coefficient is almost 80% for the submerged plate with a relative depth of 0.2. Thus, the analysis sug-

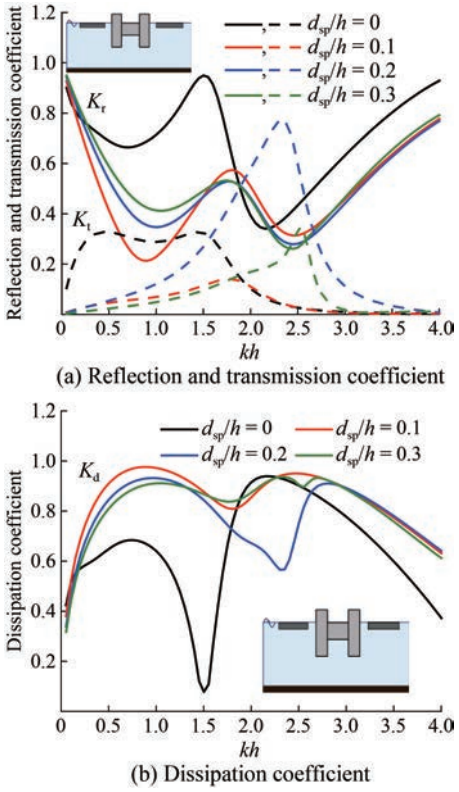

Figure 7 Variation of reflection, transmission, and dissipation coefficients versus kh for different submergence depths of plates d_{sp}/h with $d_w/h = 0.6$ and $d_f/h = 0.2$

gests that the floating plates are performing better than the submerged plates when integrated with a primary H-shaped breakwater.

Figures 8(a) and 8(b) show the variation of reflection, transmission, and dissipation coefficients versus relative spacing between the breakwater and plates w_s/λ for different plate submergence depths d_{sp}/h varying within $0 \leqslant d_{sp} \leqslant 0.3$. Similar to the results in Figures 7(a) and 7(b), the plates at the free surface are effective for better wave energy reflection. Hence, the difference in the oscillatory patterns is observed for $d_{sp}/h = 0$ and $d_{sp}/h > 0$ results in the composite structure embedded with inter-structural spacing. The peak and trough attained by K_r and K_t (Figure 8(a)) for $d_{sp}/h = 0$ has a leftward shift. A similar pattern in phase shift is found in Figure 8(b), but the composite structure $d_{sp}/h = 0$ is observed to have the lowest rate of energy dissipation. The dissipated energy has declined up to 10%, which is the lowest value of dissipation observed for lesser spacing. The dissipation coefficients experience sudden negative spikes for lower submergence depths. Thus, the noticeable performance of the breakwater integrated with plates in submerged states to dissipate the maximum amount of energy with the least transmitted wave energy for certain w_s/λ is noted, irrespective of relative submergence. The deployment of the plates under the free surface $d_{sp}/h > 0$ surpasses higher wave energy over the plates, causing a higher rate of wave transmission and significantly lower wave reflection, which leads the dissipated energy to decrease abruptly. The analysis of integrating plates in submerged conditions can offer some substantial solutions for employing the model in field conditions.

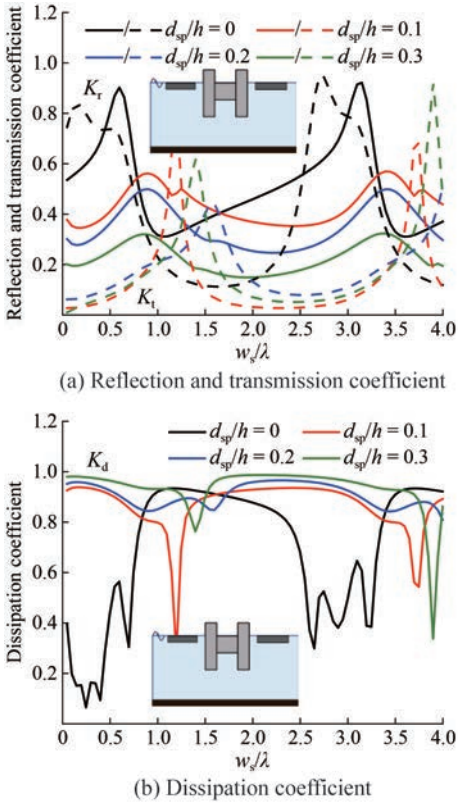

Figure 8 Variation of reflection, transmission, and dissipation coefficients versus w_s/λ for different submergence depths of plates d_{sp}/h

4.2.1.3 Effect of the width of plates

The effect of varying relative plate widths on the hydrodynamic performance is studied in Figure 9 versus nondimensional wave number kh within $0.5 \leqslant b_p/h \leqslant 2.0$. In shallow water regions $kh \leqslant 0.3$, the effect of plate width variation is observed to be insignificant, which may be due to the confined nature of wave propagation in lower water depth; hence, increasing the plate width has minimal impact on its performance. The presence of multiple structures causes the oscillatory pattern in the hydrodynamic coefficients in the intermediate-water-depth region and deep-water region. The reduced width of plates in the intermediate region $kh \leqslant 2.0$ restricts wave passage, leading to higher reflection and lower transmission, primarily driven by the resistance exerted by the seabed. In contrast, deep-water regions exhibit a reverse trend. The wider spacing between the structure and the seabed obstructs wave propagation, leading to increased reflection. This effect is further amplified for plates with larger relative widths due to enhanced wave trapping within the deeper water region

$kh \geqslant 2.0$. In Figure 9(a), the reflected wave is more than 80% by the plate with relative width $b_p/h = 2.0$ and the least energy transmitted compared to other cases, resulting in the least energy dissipation (Figure 9(a)) in the deep-water region. However, the wave trapping in the intermediate-water-depth region $1.5 \leqslant kh \leqslant 2.0$ causes a sudden drop in dissipated energy. The study shows that the composite structure is suitable in deep-water regions with higher reflected wave energy, which can be achieved with a higher relative plate width.

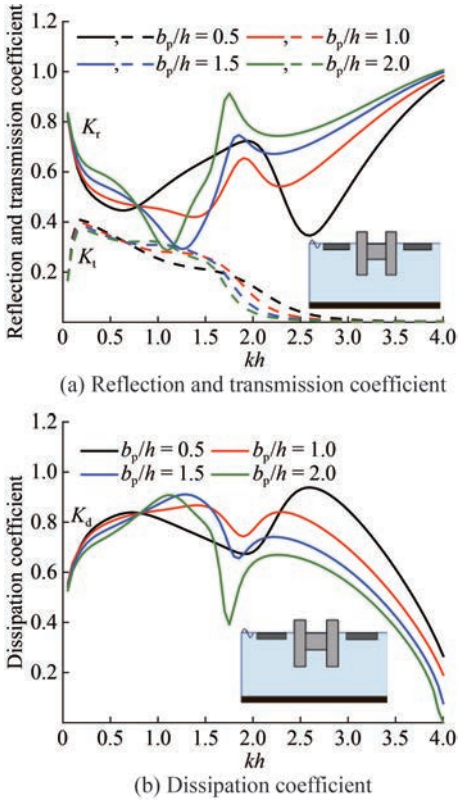

Figure 9 Variation of reflection, transmission, and dissipation coefficients versus kh for different relative widths of plates b_p/h

Similarly, the variation of K_r, K_t and K_d versus the relative spacing between the breakwater and plates w_s/λ, for different plate widths b_p/h varying within $0.5 \leqslant b_p/h \leqslant 2.0$, are depicted in Figure 10. The analysis is performed considering the intermediate-water-depth region at $kh = 2.0$. The wave energy coefficients after interaction with the composite breakwater follow an oscillatory pattern at spacing $w_s/\lambda = 2.5$ with a pair of peaks and troughs that can be observed for each case. The relative spacing between the structures stimulates the harmonic oscillations at a certain value by causing the phase shift of the maximum and minimum values. As explained in the previous case in Figure 9, the plate with higher relative width performs efficiently due to the availability of more surface area to attenuate a significant amount of wave energy. The critical relative spacing at $w_s/\lambda = 0.5$ and further spacings at each increment of $w_s/\lambda = 2.5$, the performance is inefficient due to the least reflection and highest transmission. Thus, particular spacings yield the least energy dissipation, irrespective of plate width, as observed in Figure 10(a). Hence, the spacings can be avoided during the casting of the structures in practical field applications for better performance.

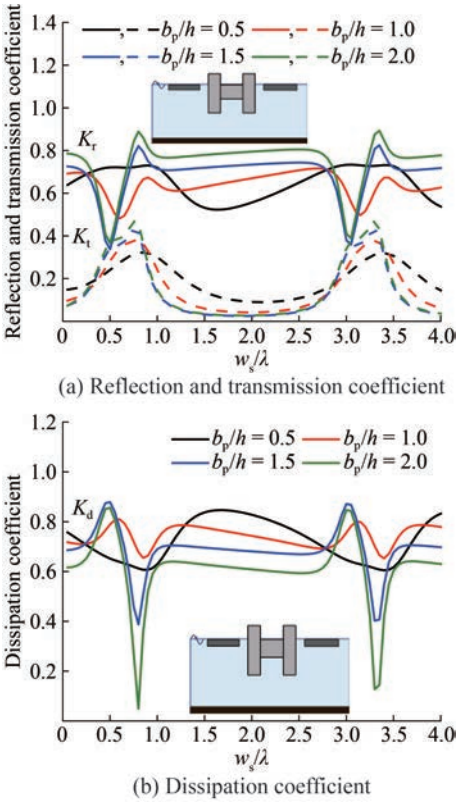

Figure 10 Variation of reflection, transmission, and dissipation coefficients versus w_s/λ for different relative widths of plates b_p/h

4.2.1.4 Effect of submergence draft of the web of H-type breakwater

Figure 11 illustrates the change in the effect of relative web draft d_w/h within $0.3 \leqslant d_w/h \leqslant 0.6$ on hydrodynamic coefficients (K_r, K_t, and K_d) for different water depths versus nondimensional wave number kh. The flange draft d_f/h is considered to vary with the web draft as the initial assumption adopted as $d_f = d_w/3$. In Figure 11(a), the reflection coefficient K_r varies directly with the web draft, as the increasing draft promotes reflecting waves by creating a vertical barrier. The increasing draft allows lesser wave energy to transmit throughout the interaction of waves in shallow and intermediate-water-depth regions ($kh \leqslant 2.0$). Furthermore, as the water depth increases, the effect of changing d_w/h becomes negligible for K_r and K_t (Figure 11(a)) and K_d (Figure 11(b)). Thus, in deeper water regions $kh \geqslant 3.0$, irrespective of d_w/h value, the structure experiences the highest reflection as well as zero transmission. The web

with the highest draft d_w/h performs as a deep barrier to encourage the reflection of bulk amount of wave energy in the intermediate-water-depth region (kh = 1.5). Therefore, the dissipated energy by the web with the highest draft is lesser compared with other cases. The oscillation in the hydrodynamic coefficient patterns is due to the presence of multiple structures and spacing between the structures. The web of an H-shaped structure promotes negative capillary action due to the presence of porous material around the surface interacting with the fluid region; hence, increasing the web depth results in more surface area and higher capillary action.

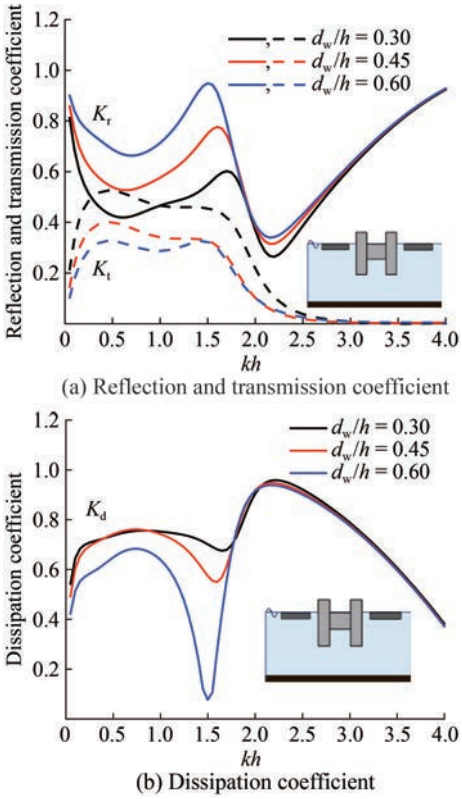

Figure 11 Variation of reflection, transmission, and dissipation coefficients versus kh for different relative drafts of the web d_w/h

The analysis for the wave transformation due to the change in the relative draft of the web d_w/h for varying relative spacing w_s/λ is performed and presented as the variation of K_r, K_t and K_d in Figure 12. The horizontal plates, when integrated with an H-shaped breakwater, have higher wave reflection and are cost-effective; hence, the study is performed for different spacing between the breakwater and plates. The spacing generates harmonic oscillations with peaks and troughs at certain values. However, the attained peak in K_r (Figure 12(a)) is higher for a higher web draft, and the trend is the opposite in K_t for a higher web draft. The peak in K_t is smooth, as the plate is less effective in restraining the transmitted wave. Hence, the peak is spiked and attains a maxima value up to 100% for the case of d_w/h = 0.6. In intermediate-water-depth regions, the higher reflection for higher web depths at certain spacings may be due to the capillary effect caused by the porous parameters. The peak followed by a trough attained by the variations is observed at w_s/λ = 2.5 in all three variations. Thus, the horizontal plate is advisable to deploy at w_s/λ = 0.5 and further spacings at each increment of w_s/λ = 2.5 with a higher d_w/h for better performance.

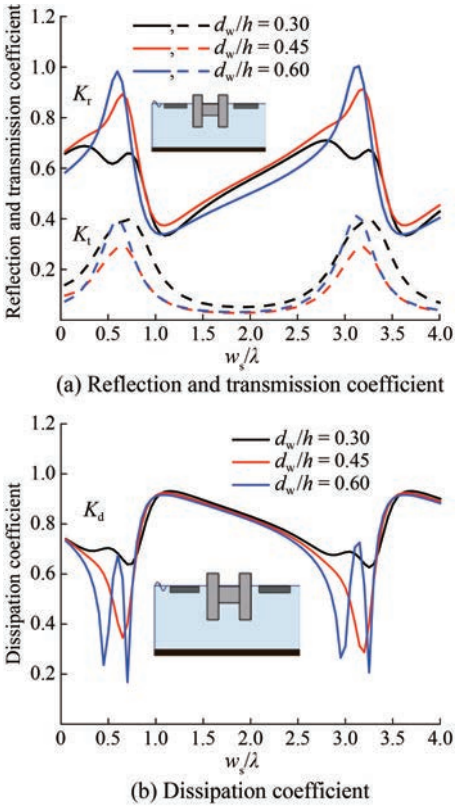

Figure 12 Variation of reflection, transmission, and dissipation coefficients versus w_s/λ for different web depths d_w/h

4.2.1.5 Effect of web width of H-type breakwater

In the previous section, the significance of the change in the submergence draft of the webs and the effect on hydrodynamic coefficients are discussed thoroughly. The thickness of the web or any other structure has a fundamental role in web attenuation as it provides robustness to the structure. Figure 13 shows the variation of the hydrodynamic coefficients (K_r, K_t and K_d) versus nondimensional wave number kh for different widths of the web of an H-shaped breakwater within $0.1 \leqslant b_w/h \leqslant 0.4$. A decreasing pattern in the reflection coefficient is noticed in the shallow water region ($kh \leqslant 0.3$), whereas an increasing pattern in K_t (Figure 13(a)) and K_d (Figure 13(b)) is observed for different widths of the web. The intermediate water region affects the reflection as it attains minima up to 20%. The minimal surface area of the slenderest web surpasses the minimum

transmitted wave in shallow and deep-water regions; hence, the web with $b_w/h = 0.1$ transmits minimum wave energy of up to 30%. The widest web offers a larger volume of porous region to transmit wave energy, which causes lesser reflected waves, hence lowering the efficiency of the breakwater. In the deep-water region, the change in the parameter is negligible on the hydrodynamic coefficients, whereas K_t vanishes in the deep-water region. The overall effect of change in the widths of the web b_w/h is less effective in terms of reflection and dissipation coefficients. Therefore, choosing a narrower web can be an effective way to reduce transmission coefficients while reflecting a maximum amount of wave energy in a cost-effective manner.

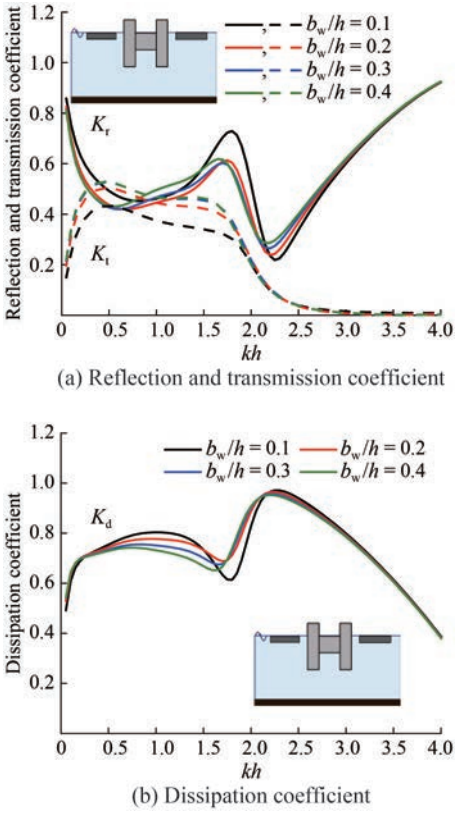

Figure 13 Variation of reflection, transmission, and dissipation coefficients versus *kh* for different web widths b_w/h

Figure 14 presents the significance of altering the web width b_w/h on varying the relative inter-spacing w_s/λ between the structures. The effects on hydrodynamic coefficients due to change in b_w/h are depicted in terms of reflection, transmission, and dissipation coefficients versus w_s/λ. The harmonic oscillatory pattern is observed in the variations with significant peaks and troughs due to the inter-spacing arrangements between the breakwater and the plates. A pair of peaks and troughs is attained in every change in $w_s/\lambda = 2.5$. Altering the values of b_w/h has no significant effect on K_r (Figure 14(a)) and K_d (Figure 14(b)). However, the attained peaks show variations in K_r and K_d, which is lower for lower b_w/h. Hence, the transmission coefficient K_t is observed to be lower for higher values of b_w/h. For certain values of spacing between the structure and plates, the transmission is at least up to 4%, as shown in Figure 14(a). The composite structure performs efficiently when the plate is deployed at $w_s/\lambda = 0.5$ and further spacings at each increment of $w_s/\lambda = 2.5$ with a higher b_w/h, which may be caused by the wider webs due to the enhanced porous volume, leading to higher wave transmission. The optimum spacing for a good performance of the structure is within $0.75 \leqslant w_s/\lambda \leqslant 1.25$, and the optimum value of relative web width is noted to be 0.4.

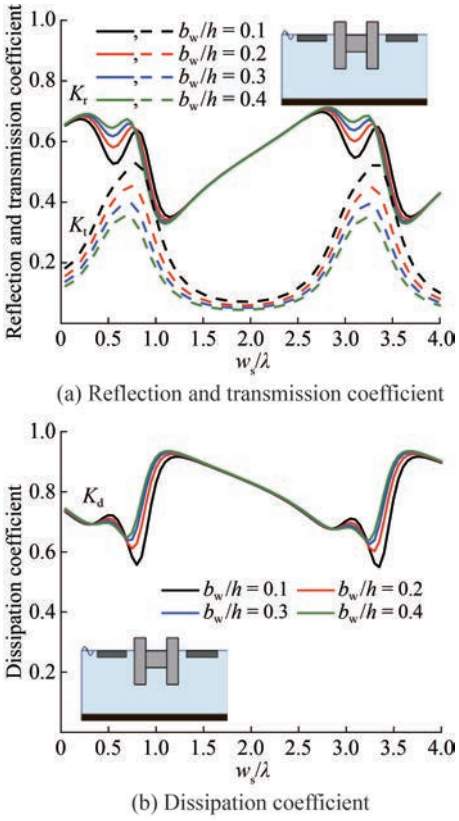

Figure 14 Variation of reflection, transmission, and dissipation coefficients versus w_s/λ for different web widths b_w/h

4.2.1.6 Effect of flange width of H-type breakwater

The H-shaped structure is composed of a flange, which helps in trapping waves, and two webs, which cause high wave reflection. Thus, the analysis is performed by changing the flange width, which is significant for different water depths and relative spacings. Figure 15 depicts the variations of K_r, K_t and K_d versus nondimensional wave number *kh* for different flange widths within $0.8 \leqslant b_f/h \leqslant 2.0$.

Considering the intermediate region, the amount of wave energy transmitted is higher than the amount of wave energy reflected, regardless of the flange width b_f/h. Because the relative flange width is higher, wave trapping is more concentrated in the structural region, resulting in higher reflection and lower transmission (Figure 15(a))

of wave energy. However, the wave trapping is noticed in the intermediate-water-depth region $0.3 \leqslant kh \leqslant 2.0$. The effect of changing the flange width is negligible in shallow and deep-water regions. The rate of energy dissipation (Figure 15(b)) is higher for the structure when changing b_f/h, irrespective of water depth. The study shows that the composite structure is suitable in deep-water regions with approximately 90% reflected wave energy, which can be achieved with the lowest relative flange width.

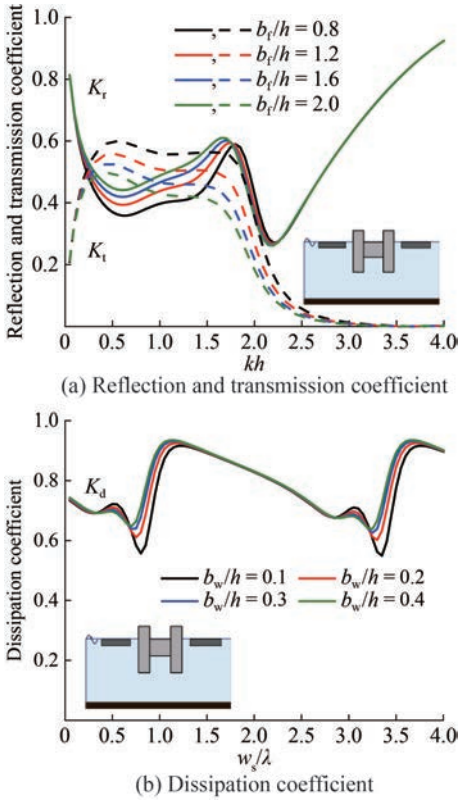

Figure 15 Variation of reflection, transmission, and dissipation coefficients versus kh for different flange widths b_f/h

The effect of flange width is studied in Figure 16 versus relative spacing between the H-shaped breakwater and structure w_s/λ for different flange widths varying within $0.8 \leqslant b_f/h \leqslant 2.0$. The pair of a crest and a trough is attained due to the spacings between the structures at every $w_s/\lambda = 2.5$. The patterns of K_r, K_t and K_d for different b_f/h is trivial. However, based on the analysis performed on varying water depths, the flange with the lowest relative width exhibits effective performance. The composite breakwater with $b_f/h = 0.8$ achieved the maximum peak value for K_r and the least value for K_t and K_d for $0.5 < w_s/\lambda < 1.0$ and $3.0 < w_s/\lambda < 3.5$. Upon changing the flange width in the intermediate-water-depth region $(kh = 2.0)$, the variation in K_t is less noticed, as observed in Figure 16(a). The composite structure is competent in dissipating a fair amount of wave energy and can be considered for practical use, as the intermediate-water-depth region is good for energy reflection and transmission, and the deep-water region is good for energy dissipation.

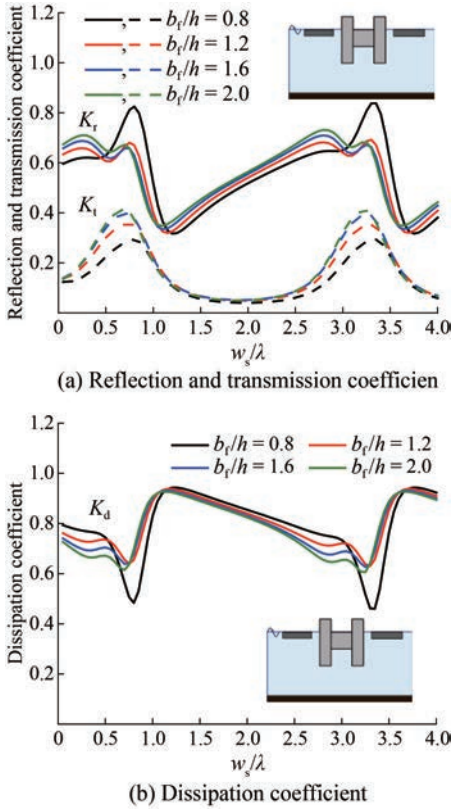

Figure 16 Variation of reflection, transmission, and dissipation coefficient versus w_s/λ for different web widths b_f/h

4.2.2 Wave force coefficients

The integrated horizontal plates with a pile-restrained H-shaped breakwater experience the incoming wave forces on the plates as well as the breakwater. In this section, the wave force coefficients are analyzed and compared for different plate porosities ε_p and different wave incident angles θ. The horizontal wave force coefficient on the seaside (i.e., facing toward the incident region) of the plate and breakwater is denoted by K_{fp} and K_{fB} (Figure 17), respectively.

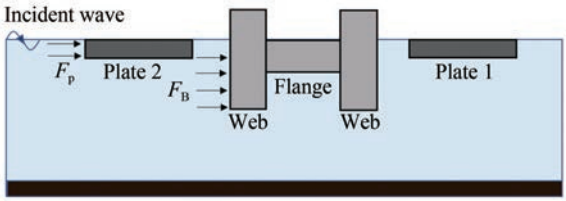

Figure 17 Wave-induced horizontal force F_p and F_B on the front side of the plate and breakwater

4.2.2.1 Effect of plate porosity

Figure 18 represents the variations of horizontal wave force coefficient on the seaside plate K_{fp} and the horizontal wave force coefficient on the seaside breakwater K_{fB} versus nondimensional wave numbers for different plate

porosities ε_p. In Figure 18(a), the variation of the horizontally projected wave force coefficient K_{fp} on the incidence face of the plate versus nondimensional wave number kh is analyzed for different porosity values within $0 \leqslant \varepsilon_p \leqslant 0.3$. Considering the impending force on the plate in the shallow water regions, the effect of changing ε_p is negligible, and a visible effect can be observed in the intermediate and deep-water regions $(kh \geqslant 2.0)$. In the intermediate water region, the impermeability of the plate with $\varepsilon_p = 0$ causes the highest value of K_{fp} on the sea side of the plate. The intensity of wave force on the plate decreases with increasing porosity, as it allows the water to pass through the structural voids. A sudden fall in K_{fp} is observed within $1.5 \leqslant kh \leqslant 2.0$ due to the spacing between the multiple structures. Figure 18(b) presents the variation of wave force on the breakwater K_{fB} for various ε_p. The performance of the structure under the action of wave force is analyzed versus nondimensional wave numbers to study the optimality of the structure in various water depth regions. The front side of the breakwater experiences a sudden increase in the wave force in the intermediate-water-depth region $1.5 < kh < 2.0$. Comparing the wave force on the plate (Figure 18(a)) and the wave force on the breakwater (Figure 18(b)), the breakwater experiences lesser force than the plate, as the majority of the wave force intensity is reduced by the presence of the plate placed at the front of the breakwater in the shallow water depth region. The composite structure experiences the highest force for the rigid plate in the intermediate region, as the combined effect of plate porosity and inter-structural spacing helps in energy dissipation. A reduction in wave force K_{fB} is observed in the deep-water region $kh \geqslant 3.0$ as the intensity of the wave force is reduced by the presence of the horizontal plate. In addition, the effect of changing the plate porosity is less significant for the wave force coefficient in shallow and intermediate-water-depth regions. The breakwater is observed to have a higher impact of wave force compared to the plate in the intermediate-water-depth region at $kh = 1.8$. Thus, the study demonstrates that the composite porous structures in deeper water experience higher wave forces compared to shallower water. This phenomenon may be due to the interaction between the plates and the waves, which disturbs the flow and consequently leads to higher energy dissipation.

4.2.2.2 Effect of angle of incidence

The effect of wave force on the plate and the breakwater is analyzed for different wave incidence angles within $0° \leqslant \theta \leqslant 60°$ versus nondimensional wave number kh in Figure 19. The variation in the wave force on the plates and the breakwater is noticeable for any water depth. In Figure 19(a), K_{fp2} is highest for $\theta = 30°$ and lowest for $\theta = 60°$ angles of incidence. In the intermediate water region, a resonating phase is obtained when the wave propagates with $\theta = 45°$ toward the structure. In the deep-water region,

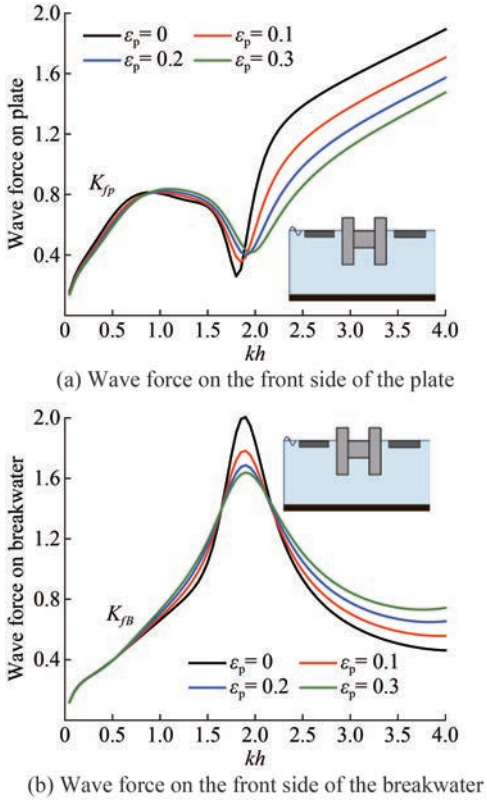

Figure 18 Variation of wave force coefficients on the front side of plate and breakwater versus kh for different plate porosities ε_p

for $kh \geqslant 3.0$, K_{fp} is highest for the normal incident wave, and it reduces as the incident angle increases. The intensity of the wave force is lowest for $\theta = 60°$ angles of incidence as the impact of wave force reduces due to the wave reflection. In the intermediate-water-depth region, K_{fp} attains minima except for $\theta = 60°$ as the wave progresses. The observation is approximately similar in Figure 19(b) in shallow water depth for K_{fB}, and resonance occurs for K_{fB} in the case of $\theta = 45°$ is very high compared to K_{fp}. The variation of wave force in the case of $\theta = 45°$ on the breakwater is significant, as the wave escapes from the plate during inclined incidence, resulting in a greater impact on the breakwater. In the deeper water depth, the breakwater encounters higher force than the plate for higher angles of incident wave.

4.3 H-type pile-restrained breakwater with inclined plates

Studies on the performance of an H-shaped breakwater integrated with a pair of inclined plates are conducted to understand the effect of the inclination of the plate on the performance of the breakwater. The study is extended to analyze the hydrodynamic coefficients and the wave forces on the structure due to the presence of inclined plates with the inclination angles varying within $0° \leqslant \alpha_{pi}, \alpha_{po} \leqslant 25°$, where α_{pi} denotes the inward inclination angle of plates

and α_{po} denotes the outward inclination angle with respect to the vertical. The schematic representation of the inclined plates and their placement with the breakwater is presented in Figure 20.

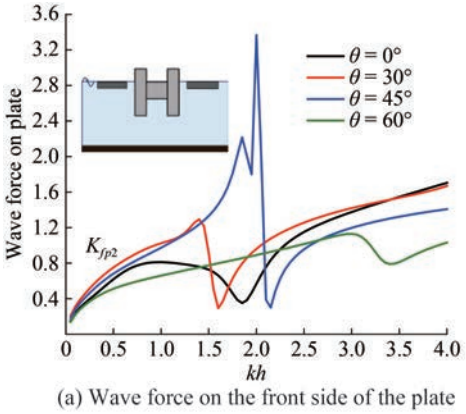

(a) Wave force on the front side of the plate

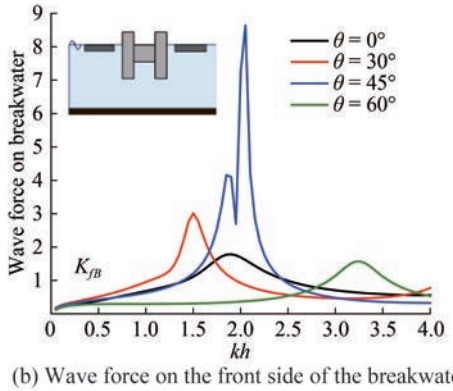

(b) Wave force on the front side of the breakwater

Figure 19 Variation of wave force coefficients on the front side of plate and breakwater versus *kh* for different angles of wave incidence θ

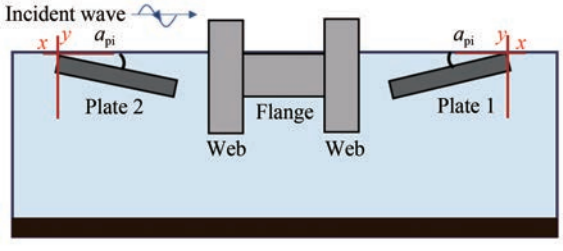

(a) H-type breakwater with inward-inclined plates

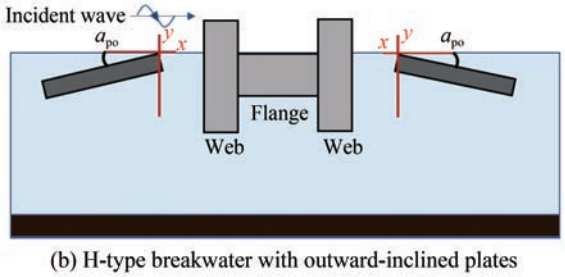

(b) H-type breakwater with outward-inclined plates

Figure 20 Composite H-type breakwater and a pair of inward- and outward-inclined plates

4.3.1 Reflection, transmission, and dissipation coefficients

The hydrodynamic performance of the composite breakwater with a pair of inclined plates in the form of reflection coefficient K_r, transmission coefficient K_t, and dissipation coefficient K_d versus nondimensional wave number *kh* and relative spacing w_s/λ is analyzed.

4.3.1.1 Inward inclination of plates

Figure 21 presents the variation of K_r, K_t and K_d versus nondimensional wave number *kh* for different inward inclinations of the plate from the free surface. The harmonic oscillation is observed due to the spacing between multiple structures, and a very high value of K_r (Figure 21(a)) is attained, which is directly proportional to the inclination angle in the shallow and deep-water region but varies inversely in the intermediate-water-depth region (Figure 21(a)). The exception can be observed for the case $\alpha_{pi} = 0°$ in both intermediate and deep-water regions as it interacts with the free surface. However, in other cases of plate inclination, the plate is partially submerged in water. Hence, due to higher inclination, the wave energy reflection rate is higher in the shallow water region $\alpha_{pi} = 25°$, exceeding 90% for K_r.

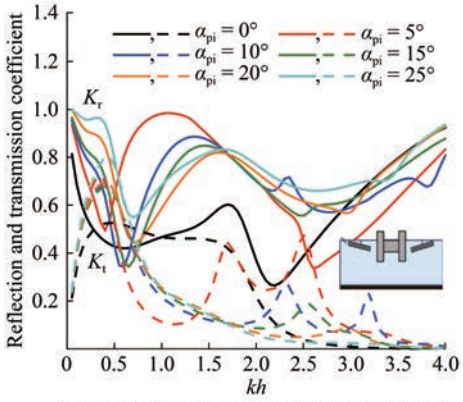

(a) Reflection and transmission coefficient

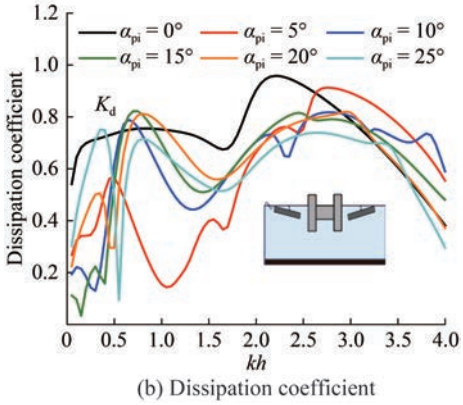

(b) Dissipation coefficient

Figure 21 Variation of reflection, transmission, and dissipation coefficients versus *kh* for different angles of inclination α_{pi}

The increasing inclination affects the reflection coefficient by creating a larger surface area of the reflecting barrier in shallow water regions; however, higher water depth causes wave trapping and makes the inclination less effec-

tive. A peculiar behavior can be observed in the oscillatory patterns of K_r (Figure 21(a)), which shows that the number of oscillations decreases with increasing angle of inclination with lower amplitude values. The rate of transmission coefficient is nearly unaffected by the variation of α_{pi} in shallow water depth. Likewise, the values for K_r and K_t variation for $\alpha_{pi} = 0°$ are different due to the exposure of the plate toward the free surface. Hence, by increasing the inclination angle, the capacity to obstruct the wave energy flow is increased, resulting in a lower transmission coefficient, as observed in Figure 21(a). The dissipation coefficient K_d (Figure 21(b)) versus kh shows that the plate at the free surface collectively dissipates higher energy, considering any water depth except the deep-water region ($kh \geqslant 3.0$).

A similar study is performed in Figure 22 to analyze the hydrodynamic coefficient versus relative spacing between breakwater and plates w_s/λ for different inclination angles of plates α_{pi}. The harmonic oscillations are observed due to multiple placed structures. In Figure 22(a), the trough attained by K_r is a minimum of up to 5% for certain values of spacing; hence, the values for w_s/λ can be ignored to get an optimum wave reflection. The attained minima for K_r and maxima for K_t are noted at every $w_s/\lambda = 2.5$ approximately. Hence, these values of spacing are not recommended to be implemented for optimum performance. The plate with an inclination angle ($\alpha_{pi} = 25°$) can be applied to get better reflection regardless of spacing and lesser transmission than any other values of α_{pi}. The dissipated energy after the wave interaction with the composite model is relatively higher than in other cases. The hydrodynamic coefficients for the plate with $\alpha_{pi} = 0°$ are different from those for the inclined plates, as observed in Figure 22. The inclined plate achieves nearly 90% or more dissipation of energy except for the inclinations at $\alpha_{pi} = 25°$. The study reveals that increasing the inclination angle in shallow water depths correlates with an increased reflection coefficient due to the increase in the reflecting barrier surface area. However, the trend loses its efficacy in deeper water regions, where wave trapping mitigates the influence of inclination.

4.3.1.2 Outward inclination of plates

This section studies the effect of outward inclination angles α_{po} on the hydrodynamic coefficient versus nondimensional wave number kh. The effect of changing α_{po} is not significant in shallow water depth ($kh \leqslant 0.3$), as shown in Figure 23. The transmission coefficient in deep-water regions ($kh \geqslant 3.0$) is also unaffected by changing the plate inclination; however, the variation of K_r is opposite as compared to K_d in deep-water regions.

A significant harmonic oscillatory pattern is observed when the waves interact in shallow and intermediate water regions. In the deep-water region, the oscillatory pattern trend gradually increases toward maxima for K_r and decreases for K_d. However, the difference is less signifi-

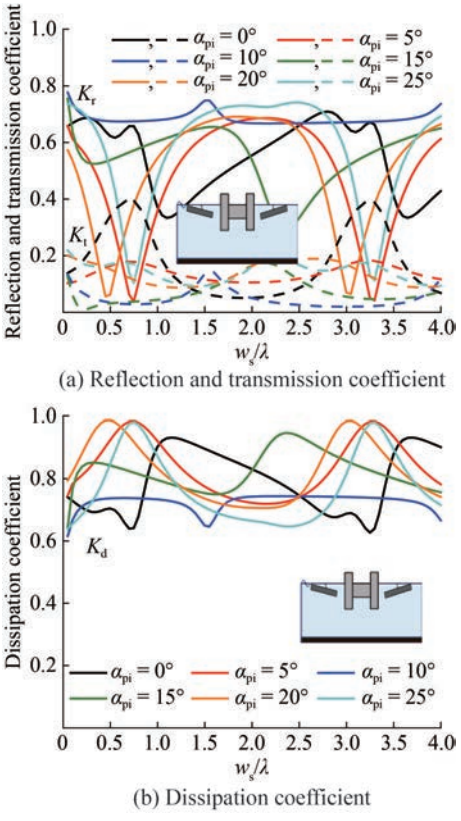

Figure 22 Variation of reflection, transmission, and dissipation coefficients versus w_s/λ for different angles of inclination α_{pi}

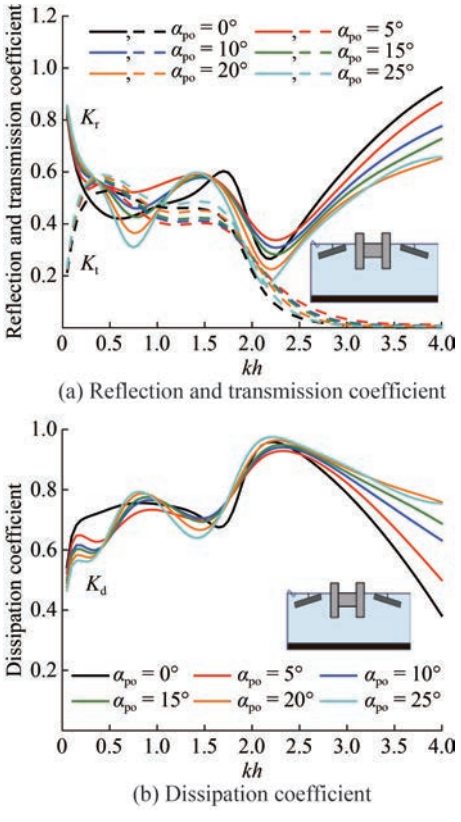

Figure 23 Variation of reflection, transmission, and dissipation coefficients versus kh for different angles of inclination α_{po}

cant; the plate with α_{po} = 5° is found to be a better arrangement for outward inclined plate integrated with a breakwater due to higher K_r and lesser K_t. The physical significance of the optimal angle for α_{po} = 5° may be due to the wave trapping caused by higher inclined plates, allowing an effective path to transmit the wave energy through the structure.

Figure 24 presents the study of the optimality of the plate inclination considering relative spacing for K_r, K_t and K_d versus w_s/λ, considering the outward inclination angle within $0° \leqslant \alpha_{po} \leqslant 25°$. The hydrodynamic coefficients are noted to behave exceptionally for the horizontally placed plate (α_{po} = 0°) due to the effect of the free surface. The outward-inclined plates reflect almost 20% less amount of wave energy when compared to a horizontally placed plate and dissipate almost 10% higher amount of wave energy than the plate for α_{po} = 0°. The difference observed in the variation of transmission characteristics is insignificant for any inclination angle, including the horizontal plate. The energy dissipation is noted to be very high, up to 95% – 100% for any inclination angle of the plate ($\alpha_{po} \geqslant 0°$). Hence, the outward inclination of the plate is less effective for reflecting a fair amount of wave energy, since a maximum of 40% energy can be reflected, and the minimum goes up to zero for certain values of spacing. Considering the variations in K_t and K_d, the outward inclined plate can be considered for effective transmission and dissipation for the proposed composite structure. Selecting the optimal plate arrangement (i.e., horizontal versus outward inclined) in intermediate water depths requires meticulous consideration of the dominance of seabed resistance over wave trapping. The findings from the analysis will help to choose the optimal configuration for desired wave reflection and energy dissipation.

4.3.2 Wave force coefficients

The variation of wave-induced force coefficients on the inclined (inward and outward) plates integrated with the H-type breakwater is presented in the following sections. The wave force effect is analyzed for different inclination angles of waves varying within $0° \leqslant \theta \leqslant 25°$, versus nondimensional wave number *kh*. The wave force coefficient is measured on the sea side of the plate placed toward the incident region, which is denoted by K_{fp}, and on the front side of the breakwater facing toward the incident region, which is denoted by K_{fB}.

Figure 25 shows the distribution of the wave force coefficients measured on the front side of the plate K_{fp} and breakwater K_{fB} versus nondimensional wave number *kh*, considering the case of the inward-inclined plate for inclination angles varying within $0° \leqslant \alpha_{pi} \leqslant 25°$. The variation of K_{fp} for a horizontal plate (α_{pi} = 0°) is slightly different than that for inclined plates. In the shallow water depth, the effect of changing α_{pi} is negligible in both K_{fp} (Figure 25(a)) and K_{fB} (Figure 25(b)). The impact of wave force on the

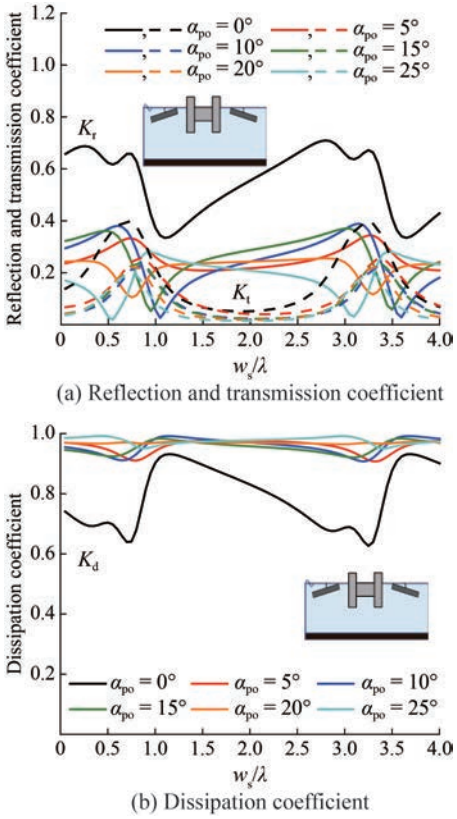

Figure 24 Variation of reflection, transmission, and dissipation coefficients versus w_s/λ for different angles of inclination α_{po}

plate gradually increases with increasing water depth, as shown in Figure 25(a). A sudden fall in K_{fp} is evident and is higher for lower inclination angles. The sudden fall in K_{fp} toward minima for α_{pi} = 5° is from 0.97 to 0.27, and for α_{pi} = 25°, the sudden fall is from 1.37 to 1.32. Hence, the plate with a higher inclination is effective in reflecting a fair amount of wave energy, but it also experiences a higher wave force due to exposure of more surface area toward the wave action. Considering the variation in K_{fB} in Figure 25(b), the wave force impact is lower for higher plate inclination. Because the majority of wave force is encountered by the plate, the effect of wave force is reduced for the breakwater, and the value of K_{fB} is lesser than K_{fp}. Hence, the attained peak in K_{fB} in Figure 25(b) is the highest for α_{pi} = 5° and lowest for α_{pi} = 25°, which is the exact opposite trend as compared with K_{fp} (Figure 25(a)) due to the exposure of more surface area toward wave action. Higher inclination angles may cause the primary reduction in wave force on the breakwater, additionally leading to other consequences like increased reflection or energy trapping. Considering the fact of reducing the impact of wave force on the breakwater, the plate with a higher inclination angle is preferable.

The variation of K_{fp} and K_{fB} is presented versus nondimensional wave number *kh* in Figure 26 for outward-inclined plates within $0° \leqslant \alpha_{po} \leqslant 25°$. The variation of K_{fp} for a hor-

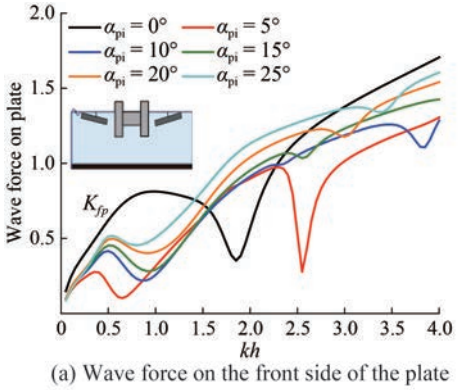

(a) Wave force on the front side of the plate

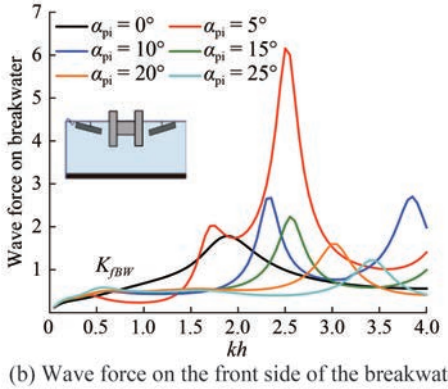

(b) Wave force on the front side of the breakwater

Figure 25 Variation of wave force coefficients on the front side of the plate and breakwater versus *kh* for different α_{pi} for inward-inclined plates

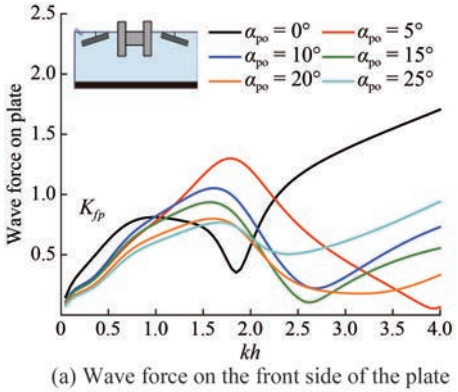

(a) Wave force on the front side of the plate

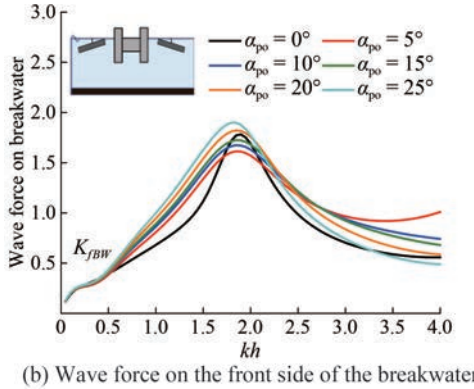

(b) Wave force on the front side of the breakwater

Figure 26 Variation of wave force coefficient for the front side of the plate and breakwater versus *kh* for different α_{po} for outward-inclined plates

izontal plate ($\alpha_{po} = 0°$) is different than in other cases of outward-inclined plates. The effect of changing α_{po} is negligible in both K_{fp} (Figure 26(a)) and K_{fB} (Figure 26(b)) in the shallow water depth. The variation is oscillatory for K_{fp}, and the plate with a lower inclination experiences higher wave force in the intermediate-water-depth region, as shown in Figure 26(a). However, an opposite trend is observed in the deep-water region and the impeded wave force is noted higher for the inclined plate. The variation of K_{fB} versus *kh* demonstrated in Figure 26(b) exhibits an opposite trend when compared to that in Figure 26(a). The induced wave force coefficient on the breakwater is more intense for the inclined plate in the intermediate-water-depth region, whereas in the deep-water region, the wave force trend is reversed. The wave force coefficient is reduced on the breakwater for both intermediate and deep-water regions if a major amount of wave energy is dissipated by the plate inclination.

5 Conclusions

A hydrodynamic analysis is performed for an H-shaped pile-restrained composite breakwater integrated with a pair of horizontal plates placed on both sides of the breakwater. The structural analysis involves the variation of porosity ε_p and submergence depth d_{sp} of the plates, width b_w and submergence draft d_w of the web, flange width b_f of the H-shaped breakwater along with the inward and outward inclination of the plates α_{pi}, α_{po} and their effect on various hydrodynamic parameters and horizontal wave force using a multidomain BEM. The numerical results are presented as functions of nondimensional wave numbers, relative inter-structural spacing between breakwater and plate, and incident wave angles. Upon analyzing the composite breakwater, the multidomain BEM is derived, and boundary conditions for the rigid horizontal seabed, free water surface condition, and incident and transmission region condition are applied. To solve the fluid-structure and structure-structure interface problems, the edge conditions are implemented. The proposed model is validated with the numerical results obtained by the existing literature. The concluding remarks drawn from this study are briefly discussed as follows:

1) The integration of a rigid horizontal plate with an H-shaped breakwater is noted to be an effective solution in deep-water regions with relative spacing varying within $1 \leqslant w_s/\lambda \leqslant 2.5$ for maximizing reflection. The change in porosity is observed to be less significant in shallow and intermediate-water-depth regions.

2) The critical wave incident angle to achieve maximum reflection and highest dissipation is noted within $40° < \theta < 60°$ accompanied by the impermeable plate of width $b_p/h = 1.0$ and spacing $w_s/h = 1.0$.

3) The plate with relative width $b_p/h = 2.0$ can reflect 90% of wave energy and transmit 10% of wave energy in

the intermediate-water-depth region.

4) The critical relative spacing at w_s/λ = 1.0 and further spacings at each increment of w_s/λ = 2.5, are favorable for obtaining the highest reflection by the composite structure.

5) The placement of the plates with any submergence depth is observed to be less effective compared to the plate interacting with the wave on the free surface.

6) The plate is advisable to be deployed at w_s/λ = 0.5 and further spacings at each increment of w_s/λ = 2.5 with d_w/h = 0.6 for optimal performance.

7) The optimum spacing for a good performance of the structure is between $0.75 \leqslant w_s/\lambda \leqslant 1.25$, and the optimum value of relative web width is noted to be 0.4.

8) The breakwater performs efficiently for the deepest web with relative depth d_w/h = 0.6 and the narrowest web with relative width b_w/h = 0.6 in the intermediate water region.

9) A significant wave force impact encountered by the impermeable plates in the deep-water region contrasts with the reduced efficacy of a plate in the intermediate water region when analysing the effects of wave force.

10) The composite structure is aligned accordingly as the impact of wave force under the incident angle θ = 45° can be reduced, or the face of the structure requires extra reinforcement to encounter the wave force impact.

11) The inclined plate achieves nearly 90% or more energy dissipation except for the inclinations at α_{pi} = 25°.

12) The energy dissipation achieved up to 95%–100% for any inclination angle of the plate ($\alpha_{po} \geqslant 0°$).

13) The outward-inclined plates reflect almost 20% less and dissipate nearly 10% higher amount of wave energy when compared to a horizontally placed plate.

14) The inclination is recommended above 5° for the arrangement of an inward-inclined plate except in deep-water regions. Aligning the plate horizontally to the free surface is more effective than using the outward-inclined plate.

15) The plate with a higher inward inclination angle $\alpha_{pi} > 5°$ is observed to reduce wave force impact on the primary structure. An outward-inclined plate is suitable only for lower inclination $\alpha_{po} < 5°$ to reduce wave impact on the breakwater.

Acknowledgement The authors are grateful to the Ministry of Education (MoE) Government of India and the National Institute of Technology Karnataka Surathkal for providing the necessary facilities for pursuing the research work. DK acknowledges the partial support from the Ministry of Ports, Shipping and Waterways, Government of India, through the research grant no. DW/01013(13)/2/2021.

Competing interest The authors have no competing interests to declare that are relevant to the content of this article.

References

Abul-Azm AG, Gesraha MR (2000) Approximation to the hydrodynamics of floating pontoons under oblique waves dual pontoon floating breakwater. Ocean Engineering 27: 365-384. https://doi.org/10.1016/S0029-8018(98)00057-2

Adee BH (1976) Floating Breakwater Performance. Ocean Engineering 159: 2777-2791. https://doi.org/10.1061/9780872620834.159

Dai J, Wang CM, Utsunomiya T, Duan W (2018) Review of recent research and developments on floating breakwaters. Ocean Engineering 158: 132-151. https://doi.org/10.1016/j.oceaneng.2018.03.083

Darlymple RA, Losada MA, Martin A (1991) Reflection and transmission from porous structure under oblique wave attack. Journal of Fluid Mechanics 224: 625-644. https://doi: 10.1017/S0022112091001908

Deng Z, Wang L, Zhao X, Huang Z (2019) Hydrodynamic performances of a T-shaped floating breakwater. Applied Ocean Research 82: 325-336. https://doi.org/10.1016/j.apor.2018.11.002

Dong GH, Zheng YN, Lia YC, Tenga B, Guanc CT, Lin DF (2008) Experiments on wave transmission coefficients of floating breakwaters. Ocean Engineering 35: 931-938. https://doi.org/10.1016/j.oceaneng.2008.01.010

Duan W, Xu S, Xu Q, Ertekin RC, Ma S (2016) Performance of an F-type floating breakwater: A numerical and experimental study. Proceedings of the Institution of Mechanical Engineers, Part M: Journal of Engineering for the Maritime Environment 231(2): 583-599. https://doi.org/10.1177/1475090216673461

Gesraha MR (2006) Analysis of Π shaped floating breakwater in oblique waves: I. Impervious rigid wave boards. Applied Ocean Research 28: 327-338. https://doi.org/10.1016/j.apor.2007.01.002

Günaydın K, Kabdaşlı MS (2004) Performance of solid and perforated U-type breakwaters under regular and irregular waves. Ocean Engineering 31: 1377-1405. https://doi.org/10.1016/j.oceaneng.2004.02.002

Günaydın K, Kabdaşlı MS (2007) Investigation of Π-type breakwaters performance under regular and irregular waves. Ocean Engineering 34: 1028-1043. https://doi.org/10.1016/j.oceaneng. 2006.03.015

Hales LZ (1981) Floating Breakwaters: State-of-the-Art Literature Review. U.S. army, corps of engineers, coastal engineering research centre Technical Report No. 81-1. https://apps. dtic. mil/sti/pdfs/ADA110692.pdf

Hu H, Wang KH, Williams AN (2002) Wave motion over a breakwater system of a horizontal plate and a vertical porous wall. Ocean Engineering 29: 373-386. https://doi.org/10.1016/S0029-8018(01)00029-4

Ji CY, Chen X, Cui J, Yuan ZM, Incecik A (2015) Experimental study of a new type of floating breakwater. Ocean Engineering 105: 295-303. https://doi.org/10.1016/j.oceaneng.2015.06.046

Koley S (2019) Wave transmission through multi-layered porous breakwater under regular and irregular incident waves. Engineering Analysis with Boundary Elements 108: 393-401. https://doi. org/10.1016/j.enganabound.2019.08.011

Kumar UV, Saha S, Bora SN (2022) Hydro-elastic analysis of a coupled porous structure in finite water depth. Ocean Engineering 246: 110491. https://doi.org/10.1016/j.oceaneng.2021.110491

Leverett MC (1941) Capillary behavior in porous solids. Transactions of AEME 142(1): 152-169. https://doi.org/10.2118/941152-G

Liu Y, Li Y, Teng B (2007) Wave interaction with a new type perforated breakwater. Acta Mechanica Sinica 23: 351-358. https://doi.org/10.1007/s10409-007-0086-1

Liu Y, Li Y, Teng B, Dong S (2008) Wave motion over a submerged breakwater with an upper horizontal porous plate and a lower horizontal solid plate. Ocean Engineering 35: 1588-1596. https://doi.org/10.1016/j.oceaneng.2008.08.003

Liu Y, Li HJ (2013) Hydrodynamic performance of a composite

breakwater with an upper horizontal porous plate and a lower rubble mound. Ocean system Engineering 3(1): 55-70. http://dx.doi.org/10.12989/ose.2013.3.1.055

Mei CC, Black JL (1969) Scattering of surface waves by rectangular obstacles in waters of finite depth. Journal of Fluid Mechanics 38(3): 499-511. https://doi.org/10.1017/S0022112069000309

Neelamani S, Rajendran R (2002a) Wave interaction with T-type breakwaters. Ocean Engineering 29: 151-175. https://doi.org/10.1016/S0029-8018(00)00060-3

Neelamani S, Vedagiri M (2002) Wave interaction with partially immersed twin vertical barriers. Ocean Engineering 29: 215-238. https://doi.org/10.1016/S0029-8018(00)00061-5

Neelamani S, Rajendran R (2002b) Wave interaction with ⊥-type breakwater. Ocean Engineering 29: 561-589. https://doi.org/10.1016/S0029-8018(01)00030-0

Nishad CS, Vijay KG, Neelamani S, Chen JT (2021) Dual BEM for wave scattering by an H-type porous barrier with nonlinear pressure drop. Engineering Analysis with Boundary Elements 131: 280-294. https://doi.org/10.1016/j.enganabound.2021.06.011

Panduranga K, Koley S (2021) Water wave trapping by floating ⊥-shaped porous breakwater. Structural Integrity and Life 21: S51-S54. http://divk.inovacionicentar.rs/ivk/ivk21/051-IVKSpecialIssue-2021-KP-SK.pdf

Patil SB, Karmakar D (2021) Performance evaluation of submerged breakwater using Multi-Domain Boundary Element Method. Applied Ocean Research 114: 102-760. https://doi.org/10.1016/j.apor.2021.102760

Twu SW, Liu CC, Hsu WH (2001) Wave damping characteristics of deeply submerged breakwaters. Journal of Waterway, Port, Coastal, Ocean Engineering 127: 97-105. https://doi.org/10.1061/(ASCE)0733-950X(2001)127:2(97)

Venkateswarlu V, Karmakar D (2020) Gravity wave trapping by series of horizontally stratified wave absorbers away from seawall. Journal of Offshore Mechanics and Arctic Engineering 142 (061201): 1-13. https://doi.org/10.1115/1.4047104

Wang K, Shi P, Chen Y, Cheng X (2019) Study on submerged upper arc-shaped plate type breakwater. China Ocean Engineering 33(2): 219-225. https://doi.org/10.1007/s13344-019-0021-9

Yip TL, Chwang AT (2000) Perforated wall breakwater with internal horizontal plate. Journal of Engineering Mechanics 126(5): 533-538. https://doi.org/10.1061/(ASCE)0733-9399(2000)126:5(533)

Yu X, Chwang AT (1994) Wave motion through porous structures. Journal of Engineering Mechanics 120: 989-1008. https://doi.org/10.1061/(ASCE)0733-9399(1994)120:5(989)

Zhan J, Chen X, Gong Y, Hu W (2017) Numerical investigation of the interaction between an inverse T-type fixed/floating breakwater and regular/irregular waves. Ocean Engineering 137: 110-119. https://doi.org/10.1016/j.oceaneng.2017.03.058

Zhang A, Li S, Cui P, Li S, Liu Y (2023) A unified theory for bubble dynamics. Physics of Fluids 35: 033323. https://doi.org/10.1063/5.0145415

Zhang C, Magee AR (2021) Effectiveness of floating breakwater in special configurations for protecting nearshore infrastructures. Journal of Marine Science and Engineering 9: 785. https://doi.org/10.3390/jmse9070785

Zhou T, Li Z (2020) Research and application of floating breakwater. International Journal of Engineering and Applied Sciences 7(6): 2394-3661. https://www.ijeas.org/download_data/IJEAS0706010.pdf